

Benchmarking of topsoil moisture estimation methods based on a field study

Sabina Thaler^{1,2*}, Josef Eitzinger¹, Milan Fischer², Gerhard Kubu¹, David Marin¹, Matěj Orság², Mirek Tnka^{2,3}, Filippo Vecchiotti⁴, Mariette Vreugdenhil⁵ and Wolfgang Wagner⁵

¹Institute of Meteorology and Climatology, BOKU University, Vienna, Austria

²Global Change Research Institute Academy of Sciences of the Czech Republic, Brno, Czech Republic

³Institute of Agriculture Systems and Bioclimatology, Mendel University in Brno, Brno, Czech Republic

⁴Department of Gravitational Natural Hazards, GeoSphere Austria, Vienna, Austria

⁵Department of Geodesy and Geoinformation, TU Wien, Vienna, Austria

Corresponding author: Sabina Thaler, sabina.thaler@boku.ac.at

Abstract

Extreme weather events caused by climate change, such as drought and heavy rainfall, will further increase in Central Europe in the near future. Resilient crop production requires in-depth knowledge of soil moisture (SM), its spatial and temporal variability and the dynamics of agriculturally used land. In the current study, different SM estimation methods, including measurement and simulation-based methods, were evaluated over a 17-ha experimental arable crop field with respect to their abilities to capture the spatial and temporal SM dynamics of within-field areas and their related uncertainty and spatial representativeness. The high spatial

This peer-reviewed article has been accepted for publication but not yet copyedited or typeset, and so may be subject to change during the production process. The article is considered published and may be cited using its DOI.

DOI: 10.1017/S0021859625000036

resolution in-situ topsoil moisture measurements (50 m grid) were compared with the estimated SM from satellite-based remote sensing (S1ASCAT) and the simulated SM from three different crop water balance models (ARIS, AquaCrop, and DSSAT). The evaluation revealed that the spatial variability in the experimental field obtained from the reference could not be captured by the alternative methods investigated because of the limitations of the grid size-related soil map information. Nevertheless, the analysis revealed a very good temporal correlation of SM dynamics with the field area average across all approaches, with AquaCrop and ARIS at a soil depth of 0–10 cm and S1ASCAT SWI 05 achieving a R^2 and a King-Gupta efficiency (KGE) > 0.80 . These results indicate the added value of complementary methods for estimating SM to reduce spatial and temporal uncertainties in the estimated topsoil water content.

Keywords: soil water content, winter wheat, remote sensing, crop growth model, in-situ measurements

Introduction

One of the most crucial resources for crop production is soil water, which is impacted by the soil, topography, vegetation, hydrology, and climatic factors (Saue and Kadaja, 2014). The soil moisture content available to plants depends on infiltrated precipitation or irrigation and the capillary rise of groundwater to the root zone, whereas the soil evaporation, drainage, runoff and plant transpiration reduce it (Allen *et al.*, 1998). Furthermore, the physical properties of soil, such as the soil pore size distribution, soil texture and structure, which can be modified by human interactions such as soil cultivation, affect the total and crop-available soil water holding capacity (Fry and Guber, 2020). A major cause of yield reductions or even crop failures in Central Europe is the insufficient availability of soil water during the growing season. These events occur mainly during the summer months (Eitzinger *et al.*, 2012a; Thaler *et al.*, 2012), with a rising trend, especially in the April–June period (Trnka *et al.*, 2020). In the coming

decades, droughts are expected to be more frequent and severe over the growing season in these regions as a result of a changing climate (Grillakis, 2019; IPCC, 2019; Hari *et al.*, 2020; Büntgen *et al.*, 2021; Ercin *et al.*, 2021; Trnka *et al.*, 2022).

Importantly, the available soil water content is highly variable both temporally and spatially (Zhang *et al.*, 2022) because of the considerable spatial variability in soil physical properties (Vanderlinden *et al.*, 2005). For precision agriculture applications, for example, monitoring the spatial variability of soil moisture (SM) at very high resolution would be highly beneficial, e.g., for increased irrigation efficiency and related crop water productivity (Vuolo *et al.*, 2017).

Currently, four different approaches are used to estimate SM for precision farming applications in croplands: direct in-situ measurements using methods such as TDR (time domain reflectometry) (Walker *et al.*, 2004); remote sensing techniques involving the use of microwave, optical and thermal sensors (Rahimzadeh-Bajgiran and Berg, 2016); non-invasive geophysical methods (Bogena *et al.*, 2015; Garré *et al.*, 2021); and soil–crop water balance modelling approaches, which are based on observed weather data (Pereira *et al.*, 2020).

Measuring the in-situ SM for different cropping systems, soils and environments is relatively costly, labour-intensive, and time-consuming (Kivi *et al.*, 2022) but is indispensable for the calibration and validation of satellite-based SM measurements, ground non-invasive geophysical methods and soil water balance models (Dorigo *et al.*, 2011). Most in-situ measurements and networks offer only low spatial representativeness. However, frequent point measurements of SM or networks of multiple stations demand high maintenance effort, which is associated with high economic costs and personnel input (Brocca *et al.*, 2017).

The use of remote sensing-based SM products over various spatial scales has been successfully applied to large areas. Here, microwave observations, either from passive or active sensors, are the most common method for measuring surface SM. The benefit of microwave remote sensing for SM estimates is the comparatively high spatio-temporal coverage in relation

to cost (Brocca *et al.*, 2017; Akash *et al.*, 2024). However, the accuracy is lower than that of in-situ measurements since remote sensing applications for SM are limited by the spatial resolution of the footprint (>10 km for most sensors except synthetic aperture radar (SAR)), the shallow penetration depth of the upper soil layer (2–7 cm), and quality issues in mountainous terrain, heavily vegetated areas and other specific surface conditions (Brocca *et al.*, 2017). At high resolutions, such as those obtained from Sentinel-1 SAR observations, soil roughness and the structure of vegetation may affect SM retrievals even more strongly than at coarse spatial scales (Vreugdenhil *et al.*, 2018). Nonetheless, the high spatio-temporal coverage of remote sensing systems cannot be reached with in-situ measurements but provides valuable insights into the large-scale dynamics of soil water fluxes. In addition to microwave sensors, thermal infrared remote sensing methods (TIRs) are also used to determine SM indirectly by assessing temperature variations (Gojiya *et al.*, 2023). While their relatively high spatial (e.g., Landsat: 30 m, Sentinel-2: 10–20 m) and temporal (e.g., Sentinel-2 every few days; Landsat with a 16-day revisit cycle) resolutions together with long-term coverage are advantages, TIR surface penetration is minimal at 1 mm and can be further limited by the density of vegetation (Rahimzadeh-Bajgiran and Berg, 2016).

Non-invasive geophysical methods, such as electrical resistivity tomography (ERT) (Shaukat *et al.*, 2024) and ground-penetrating radar (GPR) (Lu *et al.*, 2017), utilize the relationships between the SM content and the electrical properties of the soil. When SM levels change, they alter the soil conductivity and resistivity, which can be measured to infer information about the subsurface conditions (Ortuani *et al.*, 2013).

Soil water balance models of different complexities for SM estimation are cost effective and can be used for a wide range of circumstances if well calibrated. Furthermore, they are able to represent the complex interactions within soil–plant–atmosphere systems. The models can be used to simulate SM dynamics under certain boundary conditions, estimate crop yield under water shortages and find related suitable adaptation strategies, for example, to mitigate the

negative consequences of global warming on crops (Lalic *et al.*, 2018) or to optimize crop management options, such as irrigation (Naziq *et al.*, 2024). In addition to the requirement for models to be physically accurate and well representative of reality, ensuring the spatial representativeness of model input data always remains a challenge (Grassini *et al.*, 2015; Thaler *et al.*, 2018). Models still represent simplifications of rather complex interactive natural systems (Thaler *et al.*, 2012; Lalic *et al.*, 2018), and numerous modelling approaches have been explored in the past to make predictions. However, crop models need observed and measured field data, as well as field experiments, for model calibration and evaluation.

The comparison of different approaches, including field observations vs. models of several types (Palosuo *et al.*, 2011; Eitzinger *et al.*, 2012b; Rötter *et al.*, 2012) and remote sensing products (Babaeian *et al.*, 2019; Li *et al.*, 2021), provides information about the performance of these methods and highlights their strengths and weaknesses. It also offers promising options for the combined or complementary use of methods (Todoroff *et al.*, 2010; Huang *et al.*, 2019). This combination enables the following benefits: (i) Greater accuracy—By utilizing multiple data sources, a more accurate understanding of SM dynamics can be gained, leading to better agricultural practices (e.g., Zaussinger *et al.*, 2019; Lutz *et al.*, 2020; Kisekka *et al.*, 2022; Ma *et al.*, 2022). (ii) Scalability—Remote sensing offers the ability to monitor large agricultural areas, whereas in-situ measurements provide detailed insights at specific locations. Together, these methods form a scalable solution for SM assessments (Peng *et al.*, 2017; Abdulraheem *et al.*, 2023). (iii) Adapting to climate variability—As climate change impacts agricultural practices, the combined and/or complementary use of these methods allows the development of tailored adaptation options in farm practices by providing timely and reliable information on the SM status (Timlin *et al.*, 2024).

The goal of the current study was to compare and evaluate three different approaches at the crop field scale of an agricultural experimental site in northeastern Austria: (i) high-resolution measured (50 m grid) daily SM data; (ii) ASCAT and Sentinel-1 satellite data, which provide

SM levels downscaled to a 500 m grid; and (iii) simulated soil water contents from two dynamic crop growth models, AquaCrop and DSSAT (CERES-Wheat), as well as a simplified soil–plant water balance model (ARIS). All three approaches have different spatial resolutions. The specific objectives of this study were to estimate a) the spatial representativeness of the evaluated methods, b) their temporal SM dynamics, and c) their strengths and limitations as complementary methods for improving high-resolution SM estimates.

Materials and methods

Study area

The experimental field is located in Rutzendorf (48° 12' N, 16° 33' E, 150 m asl) in the northeastern part of Austria (Fig. 1b). This region, called Marchfeld, is characterized by a Pannonian climate, a distinctive continental climate belonging to the temperate zone, with warm, partly hot, and dry summers and cold winters with little snow (Thaler *et al.*, 2018). In the 17-ha experimental field, organic winter wheat was grown from 2018–2019 under rainfed conditions. The previous crop was grain peas. The sowing date was the October 22, 2018, the winter wheat was harvested on the July 5, 2019, and the yield was approximately 4600 kg/ha (mean value across the experimental field). The field was managed organically, and no fertilizer was used.

The soil type is chernozem, known for its highly variable A-horizon depth, which leads to significant local differences in the crop available water storage capacity, where the underlying C-horizon has a relatively high sand content with a relatively low available water storage capacity. The predominant spatial differences in soil texture at this trial site are shaped by the geomorphology of a terrace system with young river deposits of loess and by the former meandering of the Danube. This property leads to strong small-scale variation in the vertical soil texture characteristics in the upper soil layer of the main rooting depth of crops (up to approximately 1 m), especially with respect to the sand content, which is typical for the

Marchfeld region (Brandtner 1954). The small-scale variability within the field is clearly recognizable in the Hymap image of the studied trial field, which presents the soil surface colours determined by the sand content at the surface (Fig. 1a).

In accordance with the highest-quality soil map available from Austria “eBod” (BFW, 2024), four different soil types with available field capacities ranging from 138 mm to 220 mm up to a 1 m soil depth, as defined by Murer (1998), are summarized in the test area (Fig. 1b, Table 1).

In situ soil moisture measurements

In the first approach, a total of 65 grid points, sized 50×50 m (Fig. 1b, Parrot sensor), were set up for permanent in-situ SM measurements at a 0–10 cm soil depth during the main winter wheat growing season from April 4 to July 5, 2019. Two SM sensors, namely, Parrot sensors, were placed at each grid point and averaged for the analysis. This allowed to obtain a regular spatial distribution of SM in the topsoil. The Parrot sensors were developed by the wireless products manufacturer company Parrot SA, Paris, France, and were designed for indoor and outdoor use to provide information on potted plants. In addition to the SM, the sensor provides the near-surface air temperature, light intensity and soil fertilizer level (Parrot, 2016). The water content of the soil is measured with the capacitive method, which requires calibration with respect to the physical properties of the soil (Xaver *et al.*, 2020).

As reference samples and for calibration of the Parrot sensors, SM measurements representing a 0–10 cm soil depth, with a highly accurate handheld TDR sensor system (TRIME) (Topp *et al.*, 1980), were performed three times during the study period. All of these TDR measurements were conducted at locations where the Parrot sensors were installed, twice per location and averaged for calibration purposes (Fig. 2). The first reference data collection with the TDR sensor took place on April 4, 2019, and included 35 Parrot sensor locations within the experimental test site. Furthermore, TDR measurements of only 7 Parrot sensor locations

due to sensor failure were performed on June 1, 2019, and measurements of 59 Parrot sensor locations were performed on July 5, 2019.

Two automated agrometeorological stations with various sensors were installed in the experimental field to collect time series data on continuous weather and soil conditions at a high temporal resolution (10 min) (Fig. 1b, weather station). The first weather station (Met_01) was located within the experimental field and conducted relevant micrometeorological measurements (air temperature, global radiation, relative air humidity, and precipitation). In addition, three frequency domain reflectometer (FDR) sensors (CS616, Campbell, Logan, USA) (Robinson *et al.*, 2008) were placed vertically around the station, which presented the SM measured from a 0–30 cm soil depth (vol.%). The second agrometeorological weather station (Met_02) was situated at the western edge of the field and was equipped with the FDR-method-based sensor ECH2O EC-5 (METER Group, Munich, Germany) (METER, 2024) in a soil profile representing the SM at 10, 20, 30, 40 and 50 cm soil depths (vol.%). Air temperature, global radiation, wind speed, relative air humidity and precipitation were also measured.

Remote sensing-based SM estimates (S1ASCAT)

The second approach involved remote sensing-based SM data, which were retrieved from Metop ASCAT and Sentinel-1 active microwave observations (S1ASCAT) using the Vienna University of Technology (TU Wien) change detection method (Wagner *et al.*, 1999a,b; Naeimi *et al.*, 2009). A new vegetation parameterization was incorporated into the retrieval algorithm for Metop ASCAT, according to a previous paper (Pfeil *et al.*, 2018). The SM estimates from Metop ASCAT, with an original sampling of 12.5 km, were disaggregated to 1000 m sampling using a temporal stability approach (Wagner *et al.*, 2008; Hahn *et al.*, 2021) based on 500 m Sentinel-1 backscatter observations. This dataset is a precursor of the EUMETSAT Satellite Application Facility with the support of the Hydrology and Water Management (H SAF) disaggregated SM product H28, which was made available to the current study by TU Wien.

From the surface SM estimates, the soil–water index (SWI) was calculated. The SWI represents the SM profile at different soil depths as relative soil saturation, ranging from 0% SM at the permanent wilting point (PWP) to 100% SM at the field capacity (FC) (Brocca *et al.*, 2010; Wagner *et al.*, 2013). The SWI was calculated using the exponential filter introduced in previous papers (Wagner *et al.*, 1999a,b; Albergel *et al.*, 2008) with a characteristic time delay (T). The T value represents the smoothing of SM dynamics by infiltration, with higher T values corresponding to a higher degree of smoothing (Tong *et al.*, 2022) and representing increasing soil depths. SWI products are available daily on a 500 m grid, where the T values of 01 (SWI 01), 05 (SWI 05) and 10 (SWI10) were used for analysis in the current study. The majority of the field was covered by only one S1ASCAT grid (Fig. 3a). The adjacent grid to the east contains only three Parrot measurement points and was therefore not included in the analyses because of the low number of measured values.

Soil moisture modelling

In the third approach, daily SM was modelled using the dynamic crop growth models DSSAT-CERES-Wheat (Jones *et al.*, 2003; Hoogenboom *et al.*, 2019, 2023) and AquaCrop (Steduto *et al.*, 2008, Vanuytrecht *et al.*, 2014), as well as the GIS-based modelling system Agricultural Risk Information System (ARIS) (Eitzinger *et al.*, 2024).

The crop growth model DSSAT

The goal of the dynamic simulation model DSSAT-CERES is to comprehend the physiological mechanisms underlying plant growth at the daily simulation time step. A cultivar's growth and phenological development as a function of the photoperiod, thermal time, and dry matter distribution can only be ascertained with crop-specific genetic coefficients (Babel *et al.*, 2019; Thaler *et al.*, 2024). The functions of the initial accumulated biomass, the water and/or nitrogen stress coefficient and the actual leaf area index (LAI) provide the dry biomass at a given stage

(Deb *et al.*, 2015). The DSSAT model applies a soil water balance subroutine in which irrigation and precipitation are summed, and surface runoff, drainage, crop transpiration and soil evaporation are subtracted. Precipitation is provided by the daily weather data inputs, and irrigation is included via the experimental detail file and comprises the type of irrigation, the water supply efficiency and the date and amount of irrigation. Based on the SCS curve numbering approach (Ritchie, 1998), precipitation is split into infiltration and surface runoff. In the current study, the DSSAT version 4.8.2 was used. The input data for the model were weather, soil, genotype and management data. For this purpose, daily meteorological data from two weather stations (Met_01, Met_02) in the field were used: minimum and maximum temperatures [°C], solar radiation [MJ/m²] and precipitation [mm]. Based on the eBod soil map (BFW, 2024), four different soil type classes (Fig. 1b) were derived for the trial field (Table 1) and used as model inputs. The classes were defined by the available water capacity of the 0–1 m soil layer (Murer *et al.*, 2004) (Table 1).

The crop growth model was calibrated for winter wheat (Thaler *et al.*, 2012) and was based on the phenological components and grain yield. As the latter was only available for the entire field, the area-weighted simulated yield across all four soil types was used, with the weighting based on the proportion of area per soil class. The crop simulation was conducted from sowing on October 22, 2018 to maturity on July 5, 2019 without irrigation or fertilization.

The output of the model, which was used for the analysis, was the daily simulated SM (vol.%) of the two upper soil layers, 0–5 cm and 5–15 cm. As the in-situ measurements were conducted at a soil depth of 0–10 cm, the mean value of the two soil layers was additionally calculated to obtain a better approximation of the soil depth to the measured values (soil layer 0–10 cm).

The crop growth model AquaCrop

Like DSSAT, AquaCrop, which is based on the FAO approach (Allen *et al.*, 1998), simulates

growth processes such as biomass accumulation at daily time steps, with a focus on yield responses to water stress. As it is a generic crop model designed for irrigation planning, it uses a simplified crop growth scheme with respect to specific crop varieties or cultivar characteristics. Compared with other crop models, AquaCrop has a particular focus on water-related processes, which makes its soil module relatively detailed. It balances simplicity (to ensure usability) with a robust representation of processes such as water movement, salinity, and soil fertility dynamics, all of which influence crop growth and yield. The model estimates plant growth by calculating the daily water balance, which includes inputs such as rainfall and irrigation and outputs such as evapotranspiration (ET) and runoff. AquaCrop uses normalized water productivity and the ratio of actual crop transpiration to reference ET to determine a crop's water use efficiency (Steduto *et al.*, 2009). This information was then used to calculate the aboveground biomass. The yield is assumed to depend on the aboveground biomass and a reference harvest index, which is the ratio of the economic yield to the total aboveground biomass. Both the aboveground biomass and the harvest index must be calibrated for different crop types to ensure accurate yield predictions. This approach allows AquaCrop to simulate crop growth and yield under varying water availability and management practices (Steduto *et al.*, 2009; Vanuytrecht *et al.*, 2014; Babel *et al.*, 2019; Salman *et al.*, 2021).

The simulations were conducted using AquaCrop version 7.1. Weather, soil, crop and management data are required as input data. In addition to the daily weather data used for DSSAT (minimum and maximum temperature [°C], solar radiation [MJ/m²], and precipitation [mm]), the grass reference ET for AquaCrop was included. The soil and management data were identical to those used for DSSAT; winter wheat was calibrated using the phenology and yield data (Thaler *et al.*, 2017).

As an output, AquaCrop also has the daily simulated SM (vol.%) of the two upper soil layers 0–5 cm and 5–15 cm. Furthermore, the 0–10 cm layer was determined with the mean value of the abovementioned layers.

Agricultural Risk Information System—ARIS

The ARIS model was developed as a monitoring and forecasting tool for agricultural risk in Austria and operates at a daily time step (Eitzinger *et al.*, 2024). Compared with AquaCrop, it uses the FAO soil–crop water approach (Allen *et al.*, 1998) with a simplified calculation scheme, which is based on SoilClim (Hlavinka *et al.*, 2011). The soil–crop water module calculates daily soil–crop water balance parameters at a 500 m grid scale across Austria within a GIS scheme, including soil water depletion, related drought and heat stress impacts on crop yield and other abiotic and biotic cropping risks.

The model uses the spatial input data of various parameters such as 1 km grid-based weather data (INCA), the available soil water capacity for 2 predefined soil layers up to 1 m soil depth as a 0.5 km grid based on the eBod soil map (PWP, FC) (BFW, 2024), the CORINE Land Cover (CORINE 2018) and a digital elevation model (DEM). Thus, for the purpose of calculating the soil crop water status and crop water demand, the ARIS simulation considers the local soil and weather conditions in addition to the phenological development of the chosen crop type (Eitzinger *et al.*, 2024).

For the current study, the daily 500 m output grid “relative soil saturation” (RSS in %) was used for the test field at soil depths of 0–10 cm (RSS 0–10), 0–20 cm (RSS 0–20) and 0–40 cm (RSS 0–40) under winter wheat conditions for the analysis. Like SWI, RSS ranges from 0% SM at the PWP to 100% SM at the FC. As the values between the two grids on the field hardly differed (mean difference between 0–10 cm and 0–20 cm = 0.004%, and 0–40 cm = 0.007%), the values of the larger merged grid of 500 m size were used for the analysis (Fig. 3b).

Data compilation

High-resolution soil moisture measurements

Based on a comparison of the two sensor types, TDR and Parrot, the Parrot sensors were

calibrated with the help of a polynomial regression and subsequently validated with the measured values from the two weather stations.

Ordinary kriging was used in ArcGIS to display the spatial distribution of the Parrot point values. This geostatistical approach is widely used to generate unbiased estimates of regionalized variables in specific areas (Bayraktar and Turalioglu, 2005; Emery, 2005; Balasundra *et al.*, 2007). Ordinary kriging calculates the mean value of the variable value at a specific point (Kumar *et al.*, 2023). It relies on input data points, their positions, and spatial variation information derived from a variogram or covariance equation. These requirements are generally met effectively, even under less-than-ideal conditions (Webster and Oliver, 2007). In the current study, 65 measurements at 50×50 m spacing provided a sufficient sample size and spatial distribution for generating a reliable variogram and achieving accurate spatial interpolation. The method's ability to minimize error variance further ensures precise and unbiased predictions (Kumar *et al.*, 2023).

Remote sensing estimates and crop model simulations of soil moisture

In a further step, the SM values estimated from remote sensing (SWI), crop (vol.%) and ARIS (RSS) models were compared with the in-situ measurements and statistically evaluated. Since four soil types were simulated in the crop growth models AquaCrop and DSSAT, a spatial comparison was also possible. The simulated results were compared with the average Parrot measurements per soil type. For three Parrot measurement points (Fig. 1b), no soil data were available; they were omitted from the analysis.

For the SWI and RSS data, only one SM value was used for the entire test field because of the underlying grid size (Fig. 3); thus, only the temporal dynamics could be compared. For a statistical comparison between the different SM estimated values and the measurements of the Parrot sensors, the mean values of all the Parrot sensors within the two grids were calculated. Additionally, for the AquaCrop and DSSAT crop growth models, the area-weighted SM value

(in vol.%) of the four soil classes was calculated to obtain one daily value per model for the whole test field.

Although the in-situ measurements and AquaCrop and DSSAT simulations specify and analyse SM in vol.%, the data for the ARIS (RSS) and remote sensing-based SM values (SWI) are reported as a relationship with soil saturation [%]. The standard score (z) was applied for standardization to compare the Parrot and output values with those of the RSS and SWI units:

$$z = \frac{x - \mu}{\sigma} \quad (1)$$

where x is the raw score or observed value, μ is the mean and σ is the standard deviation.

Statistical analysis

Various statistical indicators listed below were used to compare, validate and evaluate the modelled (DSSAT, AquaCrop, and ARIS) and estimated (SWI) SM data with the measured data (Parrot).

Mean bias error (MBE): Without considering the direction of the differences, the MBE calculates the average difference between the simulated and observed values. A maximum score of 0 denotes that the simulated model is free of bias. The MBE is reported in the same units. A positive MBE indicates that the simulated values are, on average, higher than the observed values, whereas a negative MBE indicates the opposite (Janssen and Heuberger, 1995). The equation for MBE is as follows:

$$MBE = \frac{1}{n} \sum_{i=1}^n (P_i - O_i) \quad (2)$$

where n is the number of observations, P_i is the predicted value for the i -th observation and O_i is the observed value for the i -th observation.

Mean absolute error (MAE): The average of all absolute errors, presented in the same units, is known as the MAE (Willmott and Matsuura, 2005). The equation for the MAE is as follows:

$$MAE = \frac{1}{n} \sum_{i=1}^n |P_i - O_i| \quad (3)$$

where n is the number of observations, P_i is the predicted value for the i -th observation and O_i is the observed value for the i -th observation.

Root mean square error (RMSE) and unbiased RMSE (ubRMSE): The root mean square error is a widely used metric for assessing the accuracy of a model's predictions. It measures the average magnitude of the errors between the predicted values and observed values (Hyndman and Koehler, 2006). The equation for the RMSE is as follows:

$$RMSE = \frac{1}{n} \sum_{i=1}^n (P_i - O_i)^2 \quad (4)$$

where n is the number of observations, P_i is the predicted value for the i -th observation and O_i is the observed value for the i -th observation.

An alternative to the RMSE that accounts for prediction bias is the ubRMSE. It is particularly useful when the mean of the observed values is significantly different from the mean of the predicted values. The ubRMSE is calculated by removing the mean of the observed values from the predictions before computing the RMSE, which helps to provide a more accurate measure of the model's performance without the influence of systematic bias (Entekhabi *et al.*, 2010). The equation for ubRMSE is as follows:

$$ubRMSE = \sqrt{\frac{1}{n} \sum_{i=1}^n [(P_i - \bar{P}) - (O_i - \bar{O})]^2} \quad (5)$$

where n is the number of observations, P_i is the predicted value for the i -th observation, O_i is the observed value for the i -th observation, \bar{P} is the mean of the predicted values and \bar{O} is the mean of the observed values. A better model performance for both indicators is represented by a smaller value.

Kling–Gupta efficiency (KGE): The goodness-of-fit measure developed by Gupta (Gupta *et al.*, 2009) provides a diagnostic breakdown of the Nash–Sutcliffe efficiency, making it easier to analyse the relative significance of its various components (correlation, bias, and variability) in the context of hydrological modelling. The index was revised twice: once to guarantee that the bias and variability ratios are not cross-correlated (Kling *et al.*, 2012) and once to prevent

anomalously negative KGE values or values when the mean is near zero (Tang *et al.*, 2021). The range of KGE is from -Inf to 1, and the closer two sets of simulated and observed data are to 1, the more similar they are. The KGE formulation is as follows:

$$KGE = 1 - \sqrt{(r - 1)^2 + (\gamma - 1)^2 + (\beta - 1)^2} \quad (6)$$

where r is the linear correlation coefficient between the observed and predicted values, γ is the ratio of the coefficient of variation of the predicted values to the coefficient of variation of the observed values, and β is the ratio of the mean of the predicted values to the mean of the observed values.

The components are defined as follows:

$$r = \frac{\text{cov}(P, O)}{\sigma_P \sigma_O} \quad (7)$$

$$\gamma = \frac{\frac{\sigma_P}{\bar{P}}}{\frac{\sigma_O}{\bar{O}}} = \frac{\sigma_P / \bar{P}}{\sigma_O / \bar{O}} \quad (8)$$

$$\beta = \frac{\bar{P}}{\bar{O}} \quad (9)$$

where $\text{cov}(P, O)$ is the covariance between the predicted (P) and observed (O) values, σ_P is the standard deviation of the predicted values, σ_O is the standard deviation of the observed values, \bar{P} is the mean of the predicted values and \bar{O} is the mean of the observed values.

Coefficient of determination (R^2) and adjusted coefficient of determination ($\text{adj } R^2$): The percentage of the variation in the dependent variable that can be predicted from the independent variable(s) is known as the coefficient of determination (Draper and Smith, 1998). The equation for R^2 is as follows:

$$R^2 = 1 - \frac{\sum_{i=1}^n (O_i - P_i)^2}{\sum_{i=1}^n (O_i - \bar{O})^2} \quad (10)$$

where n is the number of observations, O_i is the observed value for the i -th observation, P_i is the predicted value for the i -th observation and \bar{O} is the mean of the observed values.

Although R^2 assumes that each variable explains the variation in the dependent variable, $\text{adj } R^2$ represents the percentage of variation explained by only the independent variables that

actually affect the dependent variable (Raju *et al.*, 1997).

$$adj R^2 = 1 - \left[\frac{(1-R^2)(n-1)}{n-k-1} \right] \quad (11)$$

where R^2 is the coefficient of determination, n is the number of observations and k is the number of predictors (independent variables) in the model.

Results

Calibration of the Parrot sensors

With the help of polynomial regression (Fig. 4a), the SM content from the Parrot measurements was calibrated with TDR values ($R^2 = 0.80$):

$$y = 0.021x^2 - 0.021x + 14.258 \quad (12)$$

Following calibration, the Parrot values were compared with the data obtained from the two weather stations (Fig. 4b). The closest locations of the Parrot measurements from the two weather stations were used. Located in the field centre (Fig. 1b), the Met_01 station represents the SM measurement of the 0–30 cm soil depth. With an MBE of -0.1, an RMSE of 2.97 vol.%, an MAE of 2.01 vol.%, and an R^2 of 0.84, the agreement was very high. The SM measurements at Met_02 represent a measurement at the 10 cm soil depth (horizontally suited sensor), which can be regarded as an approximated mean value for the 0–20 cm soil depth. The agreement reflects the result of Met_01 and was also very high, with an R^2 of 0.91, an RMSE of 3.99 vol.%, an MBE of -2.64 and an MAE of 3.41 vol.%.

Spatial variability

In Figure 5a, seven selected days with different levels of SM during the wheat growing season of 2019 are displayed, reflecting the seasonal precipitation pattern. At the beginning of the measurement campaign (04/2019), dry soil conditions prevailed in the field, and hardly any precipitation occurred in April (Fig. 5b). In contrast, the entire month of May experienced

intensive precipitation, which led to higher soil water contents. Individual rainfall events occurred in June, but the SM content decreased towards the end of the measurement campaign again because of the high crop water demand of a fully developed active canopy. The SM content at the study site for the entire time series can be found in the appendix (Appendix 1).

The temporal changes in the interpolated SM grid reflect the spatial soil type distribution according to the soil map relatively well, showing that the areas with the lowest SM level (corresponding to a low soil water holding capacity due to the same crop surface conditions) often remain drier in all phases of SM, except near the extreme levels (e.g., near the WP and FC). Slightly changing patterns throughout the season are caused by the interaction of soil water and nutrient storage capacity with biomass development, which in turn affect the crop transpiration rate and soil water uptake.

Time series of different soil moisture products

Soil moisture contents of the different soil types from the crop growth models

While the SM values from AquaCrop in Soils 1 and 2 agree quite well with the Parrot measurements, those in Soils 3 and 4 clearly overestimate and underestimate, respectively, the modelled SM (Fig. 6). This finding is also partly reflected in the DSSAT results, where Soil 1, Soil 2 and Soil 4 show good agreement and Soil 3 clearly overestimates. Additionally, the SM in AquaCrop at 5–15 cm is smoother and has a time lag in comparison to that in the top layer. In regard to DSSAT, this difference is less noticeable. Using the average values (0–10 cm), the simulated values could be approximated to the measured values, especially for DSSAT.

When looking at the MBE for both models at a soil depth of 0–10 cm, Soils 1 and 4 have the greatest negative deviations (Table 2). Soil 3 clearly overestimates with an MBE of 5 vol.%. Soil 2 exhibits a positive MBE in DSSAT, but it is underestimated in AquaCrop. The MAE varies from 4 to 6 vol.% for the first three soil classes; however, it is significantly higher for Soil 4, especially for AquaCrop. The ubRMSE values are the lowest for Soils 1 and 3 in

AquaCrop, as well as for Soils 1 and 4 in DSSAT, with values <4.2 vol.%. These soils also have the highest KGE values (>0.72), indicating greater similarity between the simulated and observed data. With an $\text{adj } R^2$ exceeding 0.87 for DSSAT and 0.75 for AquaCrop, the model fit was strong.

One grid-point remote sensing and crop model SM estimates vs. Parrot-measured SM

The time series and regression analysis between the measured and simulated SM (0–10 cm) using the DSSAT and AquaCrop models are shown in Fig. 7.

Both simulations closely correspond to the measured values (Fig. 7a). In AquaCrop, the simulated SM starts much higher (30.5 vol.% compared with 23 vol.% for Parrot) and then decreases to the same level as the Parrot measurements. At the beginning of May, however, the increase in SM shifts slightly and starts approximately 2 days later. A lower SM is simulated at the end of the measurement period. The $\text{adj } R^2$ value of 0.84 is high (Fig. 7b). For the AquaCrop model, an ubRMSE of 3.87 vol.%, an MBE of -0.12 vol.%, an MAE of 3.15 vol.% and a KGE of 0.87 indicate very good performance (Table 3).

Starting in April, the DSSAT displays a noticeably lower SM. By the beginning of May, it rises to 45 vol.% and reaches the same value as the Parrot measurements. The simulations in May exhibit the same curve and peaks as the measured values, but they are 2–3 vol.% overestimated. The simulated SM decreases later and reaches a lower value than the measured SM at the end of the measurement period. The $\text{adj } R^2$ of 0.89 is slightly higher than that for AquaCrop (Fig. 7b). The simulations overestimate the SM slightly (MBE = 0.82 vol.%), the MAE is 4.17 vol.%, the ubRMSE is 4.84 vol.%, and the KGE is 0.6, which indicates good performance but is slightly poorer than that of AquaCrop (Table 3).

The Parrot SM measurements with the three different RSS (ARIS model) and SWI (S1ASCAT) SM values were compared by applying mean-std scaling (z score), and the (a) time series and (b) regression analysis are presented in Fig. 8.

The Parrot measurements start in April with very dry SM values, which have a standard deviation of 0.8 that is below the mean value. On the other hand, the ARIS shows higher values at all three different soil depths. From the beginning of May, the SM increases significantly, with the RSS showing good agreement with the Parrot measurements. RSS 0–20, in particular, indicates very good correspondence up to the end of the measurement period. While the soil depth of 0–10 cm displays biased fluctuations, RSS 0–40 shows a shift in the SM values because it represents a deeper soil layer than the Parrot measurements with higher “memory”. In May, for example, the z score of RSS 0–40 increases with a delay of up to 15 days to the same value as that of Parrot, and at the end of the measurement period, it is clearly below the Parrot values. The adj R² is strong, with 0.85 for RSS 0–10, 0.83 for RSS 0–20 and 0.56 for RSS 0–40. All three simulations show an underestimation, which is most pronounced for RSS 0–40 (MBE = -0.05). The RMSE of 0.4 and the MAE of 0.32 for RSS 0–10 as well as RSS 0–20 are the lowest values. Greater deviations are observed at RSS 0–40, with an RMSE of 0.7 and an MAE of 0.58 (Table 4).

The SWI derived from S1ASCAT data shows the best agreement at SWI 05, with an adj R² of 81% (similar to ARIS RSS 0–20), and the time series is highly consistent with the Parrot values, except for some temporal overestimations. While SWI 01 has very strong fluctuations compared with the Parrot values, SWI 10 is characterized by a delay in the SM peak in May, similar to RSS 0–40, because it represents a deeper soil layer and the applied algorithm. Nevertheless, the adj R² values of 59% for SWI 01 and 63% for SWI 10 are good; the temporal course, compared with the Parrot values, fits well. The RMSE is slightly higher for RSSs between 0.4 and 0.6, the estimated SMs are overestimated (positive MBE), and the MAEs are between 0.4 and 0.5 (Table 4).

Discussion

Accurate estimates of soil water availability, for example, are crucial for assessing drought

impacts and mitigating yield loss. The interface between soil and climate determines the agricultural production potential, and understanding the SM regime is essential for identifying cropping risks and optimizing yields. However, high-resolution spatial–temporal data collection is expensive and time-consuming because of the lack of modern in-situ SM networks. As an application case in the current study, a set of actual best available databases (gridded soil map and weather datasets), modelling tools and remote sensing methods under practical conditions at a field test site in an Austrian arable region were considered. In that context, the performance of selected spatial–temporal SM estimation methods at the field scale was revealed, showing that the use of all three methods together could provide added value by checking data for errors or reliability, using them for gap filling or extending limited time series. For example, the study by Weir and Dahlhaus (2023) emphasized the lack of a continuous, accurate method for determining SM contents at the field level, which is a particular challenge for extensive dryland farming systems. Thus, combining different approaches, e.g., integrating remote sensing data into crop growth models (e.g., Ines *et al.*, 2014; Mishra *et al.*, 2021; Zhou *et al.*, 2022) or calculating different approaches and using them as an ensemble, is possible. As a result, the accuracy, robustness and flexibility of SM estimates can be improved.

Using a 65-point measurement grid (0–10 cm soil depth) in the current study, it was possible to obtain an SM value in a 50 m grid on a 17-ha winter wheat test field. This approach allowed the spatial and temporal SM dynamics for the weather conditions of the year of investigation (2019) to be visualized. Within the test field, different near-surface (0–10 cm) SM levels were observed at any time during the growing season, which depended on the spatial variation in soil conditions but also likely changed to some extent in the interaction with the spatial variation in crop biomass development and associated crop water uptake (these variations were observed but not measured). Soil properties such as the pore volume, soil texture, organic content and soil structure affect the amount and length of time the soil can store water and make nutrients available for crops and consequently define the entire growth process,

as well as the related SM regime (Huang *et al.*, 2021). Consequently, as expected, within the test field, the areas with the lowest SM content (corresponding to a low soil water holding capacity) remained frequently drier in all phases of SM, with the exception of areas near the extreme levels (e.g., near the WP and FC). These drier areas were also more affected by drought stress and presented a lower crop biomass. Despite the interactions with biomass and related crop water use, the temporal changes in the interpolated near-surface (0–10 cm) SM grid still reflect the spatial soil type distribution according to the soil map fairly well, although the soil map is related to deeper soil layers, adding some further uncertainty.

Using the AquaCrop and DSSAT crop growth models, SM was determined based on four soil classes and was thus the only approach that was also able to show spatial variability within the field. Both models exhibit similar responses to those of the measurements, with underestimations of the topsoil layer SM during dry phases and overestimations during wet phases. The 0–5 cm soil layer water content shows high sensitivity to evaporation and transpiration resulting in strong daily fluctuations in measurements as well as simulated by DSSAT and AquaCrop. The Parrot sensor measurements, however, do not show such strong peaks. The 5–15 cm soil layer, which is already part of the main rooting zone, has significant impact on crop water availability, which limits crop growth during drought periods without irrigation. The best agreement between the measured and modelled SM was achieved with AquaCrop in Soils 1 and 3 ($KGE \geq 0.78$; $adj R^2 \geq 0.88$) and with DSSAT in Soil 1 and 4 ($KGE \geq 0.73$; $adj R^2 \geq 0.9$). However, the Austrian soil map (eBod) (BFW, 2024) may have potential bias at different spatial resolutions. Even when attempting to include different soil types in the modelling tasks for the two crop models, it did not succeed in representing small-scale differences in soil conditions. Although a very sophisticated product, the Austrian soil map still has too coarse a spatial resolution for resolving within-field-scale soil property variations necessary for high-efficiency precision farming applications such as fertilization or irrigation. Furthermore, the in-situ measured data represent only the SM at the 0–10 cm soil depth, where

additional soil cultivation effects might reduce the soil water holding capacity. These temporal (seasonal) changes in the soil pore size distribution and related changes in the soil water holding capacity are not represented in the soil map or in the crop models.

The average Parrot SM values over the whole test field were compared with the 500 m grid SM values of the ARIS model, the remote sensing-based S1ASCAT-SWI product and the average SM values simulated by AquaCrop and DSSAT. This approach allows to determine which SM estimation methods are suitable for quantifying temporal SM dynamics at a resolution of 500 m. Based on the results of the statistical analysis, the data are a valuable and objective source for estimating SM in a grid of 500 m. In particular, the RSS 0–10, RSS 0–20, SWI 05, AquaCrop and DSSAT 0–10 cm are the most robust indicators of SM for the topsoil ($\text{adj } R^2 \geq 81\%$). Nevertheless, the SM estimates of SWI 01 and SWI 10 also provide valid and useful SM estimates at high temporal resolutions. The spatial and temporal resolutions of the S1ASCAT-SWI products are related to the spatial resolution of the ASCAT sensor, the assumptions of the SM algorithm and the disaggregation scheme, which together determine the final resolution of the SM product. If deeper soil layers are considered, as with RSS 0–40 or SWI 10, a shift and bias in SM can be clearly recognized. These attributes can also be observed in the two models in the 5–15 cm soil layer and are particularly pronounced in AquaCrop.

A comparison of the two crop growth models reveals that DSSAT exhibits slightly higher deviations to measured SM values than AquaCrop across the entire study area. Whereas AquaCrop underestimates the topsoil layer water content at the beginning of the study period, DSSAT shows higher values especially in May. This can be attributed to differences in the calculation of root expansion and related root water extraction over the vertical soil profile, which was not calibrated for the models in this study.

Research has shown that the direct top-down, high-spatial resolution detection of the spatial variability of SM below a “crop field” scale in the range of a few metres is currently not possible with the investigated methods S1ASCAT-SWI, large-area soil map-based crop models

(AquaCrop and DSSAT) and GIS-based (ARIS) simulations. However, in field-based precision farming applications, several methods, such as mechanized soil probing; soil surface type estimations by an RGB analysis; high spatial resolution leaf nitrogen content; sophisticated, ground-calibrated satellite products; GPS-referenced yield estimates; data-driven approaches and others (e.g., Mani *et al.*, 2020; Rayhan Shaheb *et al.*, 2022; Rozenstein *et al.*, 2023), are available to resolve spatial soil variations at a very high resolution of a few metres. The combined use of different data sources and applications may further foster the development of high spatial datasets applicable for a wide set of applications.

Nevertheless, the analysis presents a good temporal correlation at the 17-ha field-level mean SM estimates between the in-situ sensors, the S1ASCAT satellite remote sensing product and the crop model simulation results. Thus, both methods can estimate the field-level SM temporal variation quite well, which is an important step forwards in determining SM stress thresholds for crop production and is therefore an important tool for increasing the resilience and resource efficiency of cropping systems through adaptation measures, at least at the regional planning level. However, high spatial resolution in-situ sensors and remote sensing (e.g., by drones or new satellite products) for increasing either the spatial resolution of derived soil properties or direct near surface moisture will have considerable application potential for precision or smart farming techniques in the next decades.

Conclusions

In the current study, three different approaches to determine the high-resolution SM content in a winter wheat field in northeastern Austria were determined and compared: in-situ measurements, remote sensing data and model-based SM estimates. The spatial variability in the field represented by the in-situ measurements cannot be captured by the use of currently available national, sophisticated soil maps with the same spatial variation precision as the methods investigated. Even if different soil types can be used as inputs in crop models, the soil

map base data are currently not accurate enough at such a spatial resolution, as shown in the current case. Nonetheless, the analysis reveals a good temporal correlation at the mean SM level. Thus, different methods can be used to assess the temporal variation in SM contents at the field level quite well. This tool is crucial for determining the thresholds for SM stress in crop production to increase the resilience and resource efficiency of cropping systems through adaptation measures at the regional level.

Supplementary material. Appendix 1. Spatial variability of SM [vol.%] across the experimental field in Rutzendorf from 04/04/2019 until 07/05/2019, based on kriging. The dots represent the in-situ measurement points. The supplementary material for this article can be found at xxxx

Acknowledgements. This work was supported by the BMon project (project no. 872408, ASAP 14) funded by FFG, the Austrian Research Promotion Agency, Imp_DroP of the Austrian Climate Research Programme (ACRP13, project no. KR20AC0K18165), AdAgriF – Advanced methods of greenhouse gases emission reduction and sequestration in agriculture and forest landscape for climate change mitigation (CZ.02.01.01/00/22_008/0004635) and Save Water (Interreg Austria–Czechia ATCZ00048).

Author contributions. All authors contributed to the study conception and design. Data collection and material preparation were performed by JE (DSSAT, weather station Met_02), MF (weather station Met_01), GK (Parrot, GIS), DM (AquaCrop, Parrot), MO (weather station Met_01), MT (weather station Met_01), FV (GIS), MV (S1ASCAT) and WW (S1ASCAT). ST performed the modelling and statistical analysis as well as prepared the manuscript. A critical analysis of obtained results, reading and commenting of the manuscript throughout all processes were done of all authors. All authors read and approved the final manuscript.

Funding statement. This research received no specific grant from any funding agency, commercial or not-for-profit sectors.

Competing interests. The authors declare there are no conflicts of interest.

Ethical standards. Not applicable.

References

- Abdulraheem MI, Zhang W, Li S, Moshayedi AJ, Farooque AA and Hu J** (2023) Advancement of Remote Sensing for Soil Measurements and Applications: A Comprehensive Review. *Sustainability* **15**, 15444.
- Akash M, Mohan Kumar P, Bhaskar P, Deepthi PR and Sukhdev A** (2024) Review of estimation of soil moisture using active microwave remote sensing technique. *Remote Sensing Applications: Society and Environment* **33**, 101118.
- Albergel C, Rudiger C, Pellarin T, Calvet JC, Fritz N, Froissard F, Suquia D, Petitpa A, Piguet B and Martin E** (2008) From near-surface to root-zone soil moisture using an exponential filter: an assessment of the method based on in-situ observations and model simulations. *Hydrology and Earth System Sciences* **12**, 1323–1337.
- Allen R, Pereira L, Raes D and Smith M** (1998) *Crop Evapotranspiration – Guidelines for computing crop water requirements. Irrigation and Drainage Paper Nr. 56*. Rome, Italy. Available online from: <https://www.fao.org/4/X0490E/x0490e00.htm#Contents> (Accessed 7 June 2024).
- Babaeian E, Sadeghi M, Jones SB, Montzka C, Vereecken H and Tuller M** (2019) Ground, Proximal, and Satellite Remote Sensing of Soil Moisture. *Reviews of Geophysics* **57**, 530–616.

- Babel MS, Deb P and Soni P** (2019) Performance Evaluation of AquaCrop and DSSAT–CERES for Maize Under Different Irrigation and Manure Application Rates in the Himalayan Region of India. *Agricultural Research* **8**, 207–217.
- Balasundra SK, Husni MHA and Ahmed OH** (2007) Application of Geostatistical Tools to Quantify Spatial Variability of Selected Soil Chemical Properties from a Cultivated Tropical Peat. *Journal of Agronomy* **7**, 82–87.
- Bayraktar H and Turalioglu FS** (2005) A Kriging–based approach for locating a sampling site – in the assessment of air quality. *Stochastic Environmental Research and Risk Assessment* **19**, 301–305.
- BFW (Bundesforschungs– und Ausbildungszentrum für Wald Naturgefahren und Landschaft)** (2024) „eBOD“ – *Digitale Bodenkarte Österreichs*. Available online from: <https://www.bodenkarte.at> (Accessed 06 June 2024).
- Bogena HR, Huisman JA, Güntner A, Hübner C, Kusche J, Jonard F, Vey S and Vereecken H** (2015) Emerging methods for noninvasive sensing of soil moisture dynamics from field to catchment scale: a review. *Wiley Interdisciplinary Reviews–Water* **2**, 635–647.
- Brandtner F** (1954) Jungpleistozäner Löß und fossile Böden in Niederösterreich. *E&G Quaternary Science Journal* **4/5**, 49–82.
- Brocca L, Ciabatta L, Massari C, Camici S and Tarpanelli A** (2017) Soil Moisture for Hydrological Applications: Open Questions and New Opportunities. *Water* **9**, 140.
- Brocca L, Melone F, Moramarco T, Wagner W and Hasenauer S** (2010) ASCAT soil wetness index validation through in-situ and modeled soil moisture data in central Italy. *Remote Sensing of Environment* **114**, 2745–2755.
- Büntgen U, Urban O, Krusic PJ, Rybníček M, Kolář T, Kyncl T, Ač A, Koňasová E, Čáslavský J, Esper J, Wagner S, Saurer M, Tegel W, Dobrovolný P, Cherubini P,**

- Reinig F and Trnka M** (2021) Recent European drought extremes beyond Common Era background variability. *Nature Geoscience* **14**, 190–196.
- Deb P, Kiem AS, Babel MS, Chu ST and Chakma B** (2015) Evaluation of climate change impacts and adaptation strategies for maize cultivation in the Himalayan foothills of India. *Journal of Water and Climate Change* **6**, 596–614.
- Dorigo WA, Wagner W, Hohensinn R, Hahn S, Paulik C, Xaver A, Gruber A, Drusch M, Mecklenburg S, van Oevelen P, Robock A and Jackson T** (2011) The International Soil Moisture Network: a data hosting facility for global in-situ soil moisture measurements. *Hydrology and Earth System Sciences* **15**, 1675–1698.
- Draper NR and Smith H** (1998) On Worthwhile Regressions, Big F's, and R². In *Applied Regression Analysis*. Wiley Series in Probability and Statistics, Hoboken, USA, 3. Edition, 243–250.
- Eitzinger J, Kersebaum KC and Formayer H** (2009) *Landwirtschaft im Klimawandel. Auswirkungen und Anpassungsstrategien für die Land- und Forstwirtschaft in Mitteleuropa*. Agrimedia, Clenze, Germany, 1. Edition.
- Eitzinger J, Trnka M, Semerádová D, Thaler S, Svobodová E, Hlavinka P, Šiška B, Takáč J, Malatinská L, Nováková M, Dubrovský M and Žalud Z** (2012a) Regional climate change impacts on agricultural crop production in Central and Eastern Europe – hotspots, regional differences and common trends. *The Journal of Agricultural Science* **151**, 787–812.
- Eitzinger J, Thaler S, Schmid E, Strauss F, Ferrise R, Moriondo M, Bindi M, Palosuo T, Rötter R, Kersebaum KC, Olesen JE, Patil RH, Şaylan L, Çaldağ B and Çaylak O** (2012b) Sensitivities of crop models to extreme weather conditions during flowering period demonstrated for maize and winter wheat in Austria. *The Journal of Agricultural Science* **151**, 813–835.

- Eitzinger J, Daneu V, Kubu G, Thaler S, Trnka M, Schaumberger A, Schneider S and Tran TMA** (2024) Grid based monitoring and forecasting system of cropping conditions and risks by agrometeorological indicators in Austria – Agricultural Risk Information System ARIS. *Climate Services* **34**, 100478.
- Emery X** (2005) Simple and ordinary multigaussian kriging for estimating recoverable reserves. *Mathematical Geology* **37**, 295–319.
- Entekhabi D, Reichle RH, Koster RD and Crow WT** (2010) Performance Metrics for Soil Moisture Retrievals and Application Requirements. *Journal of Hydrometeorology* **11**, 832–840.
- Ercin E, Veldkamp TIE and Hunink J** (2021) Cross–border climate vulnerabilities of the European Union to drought. *Nature Communications* **12**, 3322.
- Fry JE and Guber AK** (2020) Temporal stability of field–scale patterns in soil water content across topographically diverse agricultural landscapes. *Journal of Hydrology* **580**, 124260.
- Garré S, Hyndman D, Mary B and Werban U** (2021) Geophysics conquering new territories: The rise of “agrogeophysics”. *Vadose Zone Journal* **20**, e20115.
- Gojiya K, Rank DH, Chauhan P, Patel D, Satasiya RM and Girish P** (2023) Advances in Soil Moisture Estimation through Remote Sensing and GIS: A Review. *International Research Journal of Modernization in Engineering Technology and Science* **5**, 2669–2678.
- Grassini P, van Bussel LGJ, Van Wart J, Wolf J, Claessens L, Yang H, Boogaard H, de Groot H, van Ittersum MK and Cassman KG** (2015) How good is good enough? Data requirements for reliable crop yield simulations and yield–gap analysis. *Field Crops Research* **177**, 49–63.
- Grillakis MG** (2019) Increase in severe and extreme soil moisture droughts for Europe under climate change. *Science of The Total Environment* **660**, 1245–1255.

- Gupta HV, Kling H, Yilmaz KK and Martinez GF** (2009) Decomposition of the mean squared error and NSE performance criteria: Implications for improving hydrological modelling. *Journal of Hydrology* **377**, 80–91.
- Hahn S, Wagner W, Steele–Dunne SC, Vreugdenhil M and Melzer T** (2021) Improving ASCAT Soil Moisture Retrievals With an Enhanced Spatially Variable Vegetation Parameterization. *IEEE Transactions on Geoscience and Remote Sensing* **59**, 8241–8256.
- Hari V, Rakovec O, Markonis Y, Hanel M and Kumar R** (2020) Increased future occurrences of the exceptional 2018–2019 Central European drought under global warming. *Scientific Reports* **10**, 12207.
- Hlavinka P, Trnka M, Balek J, Semerádová D, Hayes M, Svoboda M, Eitzinger J, Možný M, Fischer M, Hunt E and Žalud Z** (2011) Development and evaluation of the SoilClim model for water balance and soil climate estimates. *Agricultural Water Management* **98**, 1249–1261.
- Hoogenboom G, Porter CH, Boote KJ, Shelia V, Wilkens PW, Singh U, White JW, Asseng S, Lizaso JI, Moreno LP, Pavan W, Ogoshi RM, Hunt LA, Tsuji GY and Jones JW** (2019) The DSSAT crop modeling ecosystem. In Boote KJ (Editor) *Advances in Crop Modeling for a Sustainable Agriculture*. Burleigh Dodds Science Publishing, Cambridge, United Kingdom, 173–216.
- Hoogenboom G, Porter CH, Shelia V, Boote KJ, Singh U, White JW, Pavan W, Oliveira FAA, Moreno–Cadena LP, Lizaso JI, Asseng S, Pequeno DNL, Kimball BA, Alderman PD, Thorp KR, Jones MR, Cuadra SV, Vianna MS, Villalobos FJ, Ferreira TB, Batchelor WD, Koo J, Hunt LA and Jones JW** (2023) *Decision Support System for Agrotechnology Transfer (DSSAT) Version 4.8.2 (www.dssat.net)*. DSSAT Foundation, Gainesville, Florida, USA.

- Huang J, Gómez-Dans JL, Huang H, Ma H, Wu Q, Lewis PE, Liang S, Chen Z, Xue J-H, Wu Y, Zhao F, Wang J and Xie X** (2019) Assimilation of remote sensing into crop growth models: Current status and perspectives. *Agricultural and Forest Meteorology* **276–277**, 107609.
- Huang J, Hartemink AE and Kucharik CJ** (2021) Soil-dependent responses of US crop yields to climate variability and depth to groundwater. *Agricultural Systems* **190**, 103085.
- Hyndman RJ and Koehler AB** (2006) Another look at measures of forecast accuracy. *International Journal of Forecasting* **22**, 679–688.
- Ines AVM, Das NN, Hansen JW and Njoku EG** (2013) Assimilation of remotely sensed soil moisture and vegetation with a crop simulation model for maize yield prediction. *Remote Sensing of Environment* **138**, 149–164.
- IPCC** (2019) Shukla PR, Skea J, Calvo Buendia E, Masson-Delmotte V, Pörtner H-O, Roberts DC, Zhai P, Slade R, Connors S, van Diemen R, Ferrat M, Haughey E, Luz S, Neogi S, Pathak M, Petzold J, Portugal Pereira J, Vyas P, Huntley E, Kissick K, Belkacemi M and Malley J (Eds). *Climate Change and Land: an IPCC special report on climate change, desertification, land degradation, sustainable land management, food security, and greenhouse gas fluxes in terrestrial ecosystems*. Available online from: <https://www.ipcc.ch/srccl/> (Accessed 7 June 2024).
- Janssen PHM and Heuberger PSC** (1995) Calibration of Process-Oriented Models. *Ecological Modelling* **83**, 55–66.
- Jones JW, Hoogenboom G, Porter CH, Boote KJ, Batchelor WD, Hunt LA, Wilkens PW, Singh U, Gijsman AJ and Ritchie JT** (2003) The DSSAT cropping system model. *European Journal of Agronomy* **18**, 235–265.
- Kisekka I, Peddinti SR, Kustas WP, McElrone AJ, Bambach-Ortiz N, McKee L and Bastiaanssen W** (2022) Spatial-temporal modeling of root zone soil moisture dynamics

in a vineyard using machine learning and remote sensing. *Irrigation Science* **40**, 761–777.

Kivi M, Vergopolan N and Dokoochaki H (2022) A comprehensive assessment of in-situ and remote sensing soil moisture data assimilation in the APSIM model for improving agricultural forecasting across the U.S. Midwest. *Hydrology and Earth System Sciences Discussions* **2022**, 1–33.

Kling H, Fuchs M and Paulin M (2012) Runoff conditions in the upper Danube basin under an ensemble of climate change scenarios. *Journal of Hydrology* **424–425**, 264–277.

Kumar P, Rao B, Burman A, Kumar S and Samui P (2023) Spatial variation of permeability and consolidation behaviors of soil using ordinary kriging method. *Groundwater for Sustainable Development* **20**, 100856.

Lalic B, Firanj Sremac A, Eitzinger J, Stricevic R, Thaler S, Maksimovic I, Danicic M, Perisic D and Dekic L (2018) Seasonal forecasting of green water components and crop yield of summer crops in Serbia and Austria. *The Journal of Agricultural Science* **156**, 658–672.

Li Z–L, Leng P, Zhou C, Chen K–S, Zhou F–C and Shang G–F (2021) Soil moisture retrieval from remote sensing measurements: Current knowledge and directions for the future. *Earth–Science Reviews* **218**, 103673.

Lu Y, Song W, Lu J, Wang X and Tan Y (2017) An Examination of Soil Moisture Estimation Using Ground Penetrating Radar in Desert Steppe. *Water* **9**, 521.

Lutz F, Del Grosso S, Ogle S, Williams S, Minoli S, Rolinski S, Heinke J, Stoorvogel JJ and Müller C (2020) The importance of management information and soil moisture representation for simulating tillage effects on N₂O emissions in LPJmL5.0–tillage. *Geoscientific Model Development* **13**(9), 3905–3923.

- Ma B, Wang Q, Xue B, Hou Z, Jiang Y and Cai W** (2022) Application of UAV Remote Sensing in Monitoring Water Use Efficiency and Biomass of Cotton Plants Adjacent to Shelterbelt. *Frontiers in Plant Science* **13**, 894172.
- Mani PK, Mandal A, Biswas S, Sarkar B, Mitran T and Meena R** (2020) Remote Sensing and Geographic Information System: A Tool for Precision Farming. In Mitran T, Meena RS and Chakraborty A (eds) *Geospatial Technologies for Crops and Soils*. Springer, Singapore.
- Mehrabi F and Sepaskhah AR** (2020) Winter Wheat Yield and DSSAT Model Evaluation in a Diverse Semi-Arid Climate and Agronomic Practices. *International Journal of Plant Production* **14**, 221-243.
- METER** (2024) *ECH2O EC-5 Soil Moisture Sensor*. Available online from <https://metergroup.com/products/ech20-ec-5-soil-moisture-sensor/> (Accessed 7 June 2024).
- Mishra V, Cruise JF and Mecikalski JR** (2021) Assimilation of coupled microwave/thermal infrared soil moisture profiles into a crop model for robust maize yield estimates over Southeast United States. *European Journal of Agronomy* **123**, 126208.
- Murer E** (1998) Die Ableitung der Parameter eines Bodenwasserhaushalts- und Stofftransportmodelles aus den Ergebnissen der Bodenkartierung. Modelle für die gesättigte und ungesättigte Bodenzone. *Schriftenreihe BAW* **7**, 89–103.
- Murer E, Wagenhofer J, Aigner F and Pfeffer M** (2004) Die nutzbare Feldkapazität der mineralischen Böden der landwirtschaftlichen Nutzfläche Österreichs. *Schriftenreihe BAW* **20**, 72–78.
- Naeimi V, Bartalis Z and Wagner W** (2009) ASCAT Soil Moisture: An Assessment of the Data Quality and Consistency with the ERS Scatterometer Heritage. *Journal of Hydrometeorology* **10**, 555–563.

- Naziq MS, Sathyamoorthy NK, Ga D, Pazhanivelan S and Vadivel N** (2024) Coupled weather and crop simulation modeling for smart irrigation planning: a review. *Water Supply* **24**(8), 2844–2865.
- Oleson KW, Lawrence DM, Bonan G, Flanner M, Kluzek E, Lawrence P, Levis S, Swenson S, Thornton P and Dai A** (2010) Technical description of version 4.0 of the Community Land Model (CLM), NCAR Tech. Notes (NCAR/TN-478+ STR).
- Ortuani B, Benedetto A, Giudici M, Mele M and Tosti F** (2013) A Non-invasive Approach to Monitor Variability of Soil Water Content with Electromagnetic Methods. *Procedia Environmental Sciences* **19**, 446–455.
- Palosuo T, Kersebaum KC, Angulo C, Hlavinka P, Moriondo M, Olesen JE, Patil RH, Ruget F, Rumbaur C, Takáč J, Trnka M, Bindi M, Çaldağ B, Ewert F, Ferrise R, Mirschel W, Şaylan L, Šiška B and Rötter R** (2011) Simulation of winter wheat yield and its variability in different climates of Europe: A comparison of eight crop growth models. *European Journal of Agronomy* **35**, 103–114.
- Parrot** (2016) *Parrot Flower Power. User guide*. Available online from: https://www.parrot.com/assets/s3fs-public/2021-09/flower-power_user-guide_uk.pdf (Accessed 7 June 2024).
- Peng J, Loew A, Merlin O and Verhoest NEC** (2017) A review of spatial downscaling of satellite remotely sensed soil moisture. *Reviews of Geophysics* **55**, 341–366.
- Pereira LS, Paredes P and Jovanovic N** (2020) Soil water balance models for determining crop water and irrigation requirements and irrigation scheduling focusing on the FAO56 method and the dual Kc approach. *Agricultural Water Management* **241**, 106357.
- Pfeil I, Vreugdenhil M, Hahn S, Wagner W, Strauss P and Blöschl G** (2018) Improving the Seasonal Representation of ASCAT Soil Moisture and Vegetation Dynamics in a Temperate Climate. *Remote Sensing* **10**, 1788.

- Rahimzadeh–Bajgiran P and Berg A** (2016) Chapter 3 – Soil Moisture Retrievals Using Optical/TIR Methods. In Srivastava PK, Petropoulos GP and Kerr YH (eds) *Satellite Soil Moisture Retrieval*. Elsevier, Amsterdam, Netherlands, Oxford, UK, Cambridge, USA, 47–72.
- Raju NS, Bilgic R, Edwards JE and Fleer PF** (1997) Methodology Review: Estimation of Population Validity and Cross–Validity, and the Use of Equal Weights in Prediction. *Applied Psychological Measurement* **21**, 291–305.
- Rayhan Shaheb M, Sarker A and Shearer SA** (2022) Chapter 4. Precision Agriculture for Sustainable Soil and Crop Management. In Michael A and Indi B (eds) *Soil Science – Emerging Technologies, Global Perspectives and Applications*. IntechOpen, London, UK, 49–72.
- Ritchie JT** (1998) Soil water balance and plant water stress. In Tsuji GY, Hoogenboom G and Thornton PK (Eds) *Understanding Options for Agricultural Production*. Springer Netherlands, Dordrecht, Netherlands, 41–54.
- Robinson DA, Campbell CS, Hopmans JW, Hornbuckle BK, Jones SB, Knight R, Ogden F, Selker J and Wendroth O** (2008) Soil Moisture Measurement for Ecological and Hydrological Watershed–Scale Observatories: A Review. All rights reserved. No part of this periodical may be reproduced or transmitted in any form or by any means, electronic or mechanical, including photocopying, recording, or any information storage and retrieval system, without permission in writing from the publisher. *Vadose Zone Journal* **7**, 358–389.
- Rötter RP, Palosuo T, Kersebaum KC, Angulo C, Bindi M, Ewert F, Ferrise R, Hlavinka P, Moriondo M, Nendel C, Olesen JE, Patil RH, Ruget F, Takáč J and Trnka M** (2012) Simulation of spring barley yield in different climatic zones of Northern and Central Europe: A comparison of nine crop models. *Field Crops Research* **133**, 23–36.

- Rozenstein O, Cohen Y, Alchanatis V, Behrendt K, Bonfil DJ, Eshel G, Harari A, Harris WE, Klapp I, Laor Y, Linker R, Paz–Kagan T, Peets S, Rutter SM, Salzer Y and Lowenberg–DeBoer J** (2023) Data–driven agriculture and sustainable farming: friends or foes? *Precision Agriculture* **25**, 520–531.
- Salman M, García–Vila M, Fereres E, Raes D and Steduto P** (2021) *The AquaCrop model – Enhancing crop water productivity: Ten years of development, dissemination and implementation 2009–2019. FAO Water Report No. 47*. FAO, Rome, Italy. Available online from: <https://openknowledge.fao.org/items/890f6033–554e–4e48–8dbb–5f1d809536e2> (Accessed 7 June 2024).
- Saue T and Kadaja J** (2014) Water limitations on potato yield in Estonia assessed by crop modelling. *Agricultural and Forest Meteorology* **194**, 20–28.
- Shaukat H, Flower KC and Leopold M** (2024) Comparing quasi–3D soil moisture derived from electromagnetic induction with 1D moisture sensors and correlation to barley yield in variable duplex soil. *Soil and Tillage Research* **236**, 105953.
- Steduto P, Hsiao TC, Raes D and Fereres E** (2009) AquaCrop–The FAO Crop Model to Simulate Yield Response to Water: I. Concepts and Underlying Principles. *Agronomy Journal* **101**, 426–437.
- Steduto P, Raes D, Hsiao TC, Fereres E, Heng L, Izzi G and Hoogeveen J** (2008) AquaCrop: A New Model for Crop Prediction Under Water Deficit Conditions. *Options Méditerranéennes, Series A*, **80**, 285–292.
- Tang G, Clark MP and Papalexiou SM** (2021). SC–Earth: A Station–Based Serially Complete Earth Dataset from 1950 to 2019. *Journal of Climate* **34**, 6493–6511.
- Thaler S, Berger K, Eitzinger J, Mahnaz A, Shala–Mayrhofer V, Zamini S and Weihs P** (2024) Radiation Limits the Yield Potential of Main Crops Under Selected Agrivoltaic Designs—A Case Study of a New Shading Simulation Method. *Agronomy* **14**, 2511.

- Thaler S, Eitzinger J, Trnka M and Dubrovsky M** (2012) Impacts of climate change and alternative adaptation options on winter wheat yield and water productivity in a dry climate in Central Europe. *The Journal of Agricultural Science* **150**, 537–555.
- Thaler S, Eitzinger J, Trnka M, Možný M, Hahn S, Wagner W and Hlavinka P** (2018) The performance of Metop Advanced SCATterometer soil moisture data as a complementary source for the estimation of crop–soil water balance in Central Europe. *The Journal of Agricultural Science* **156**, 577–598.
- Thaler S, Gobin A and Eitzinger J** (2017) Water Footprint of main crops in Austria / Wasser–Fußabdruck wichtiger Nutzpflanzen in Österreich. *Die Bodenkultur: Journal of Land Management, Food and Environment* **68**, 1–15.
- Timlin D, Paff K and Han E** (2024) The role of crop simulation modeling in assessing potential climate change impacts. *Agrosystems, Geosciences & Environment* **7**, e20453.
- Todoroff P, De Robillard F and Laurent JB** (2010) Interconnection of a crop growth model with remote sensing data to estimate the total available water capacity of soils. *2010 IEEE International Geoscience and Remote Sensing Symposium*, 1641–1644.
- Tong R, Parajka J, Széles B, Greimeister–Pfeil I, Vreugdenhil M, Komma J, Valent P and Blöschl G** (2022) The value of satellite soil moisture and snow cover data for the transfer of hydrological model parameters to ungauged sites. *Hydrology and Earth System Sciences* **26**, 1779–1799.
- Topp GC, Davis JL and Annan AP** (1980) Electromagnetic determination of soil water content: Measurements in coaxial transmission lines. *Water Resources Research* **16**, 574–582.
- Trnka M, Hlavinka P, Možný M, Semerádová D, Štěpánek P, Balek J, Bartošová L, Zahradníček P, Blahová M, Skalák P, Farda A, Hayes M, Svoboda M, Wagner W, Eitzinger J, Fischer M and Zalud Z** (2020) Czech Drought Monitor System for

monitoring and forecasting agricultural drought and drought impacts. *International Journal of Climatology* **40**, 5941–5958.

- Trnka M, Vizina A, Hanel M, Balek J, Fischer M, Hlavinka P, Semerádová D, Stepánek P, Zahradníček P, Skalák P, Eitzinger J, Dubrovsky M, Máca P, Belínová M, Zeman E and Brázdil R** (2022) Increasing available water capacity as a factor for increasing drought resilience or potential conflict over water resources under present and future climate conditions. *Agricultural Water Management* **264**, 107460.
- Vanderlinden K, Giráldez JV and Van Meirvenne M** (2005) Soil Water-Holding Capacity Assessment in Terms of the Average Annual Water Balance in Southern Spain. *Vadose Zone Journal* **4**, 317-328.
- Vanuytrecht E, Raes D, Steduto P, Hsiao TC, Heng LK, Vila MG, Moreno PM and Moreno PM** (2014) AquaCrop: FAO's crop water productivity and yield response model. *Environmental Modelling & Software* **62**, 351–360.
- Vreugdenhil M, Wagner W, Bauer–Marschallinger B, Pfeil I, Teubner I, Rüdiger C and Strauss P** (2018) Sensitivity of Sentinel–1 Backscatter to Vegetation Dynamics: An Austrian Case Study. *Remote Sensing* **10**, 1396.
- Vuolo F, Essl L, Zappa L, Sandén T and Spiegel H** (2017) Water and nutrient management: the Austria case study of the FATIMA H2020 project. *Advances in Animal Biosciences* **8**, 400–405.
- Wagner W, Hahn S, Kidd R, Melzer T, Bartalis Z, Hasenauer S, Figa–Saldaña J, de Rosnay P, Jann A, Schneider S, Komma J, Kubu G, Brugger K, Aubrecht C, Züger J, Gangkofner U, Kienberger S, Brocca L, Wang Y, Blöschl G, Eitzinger J, Steinnocher K, Zeil P and Rubel F** (2013) The ASCAT Soil Moisture Product: A Review of its Specifications, Validation Results, and Emerging Applications. *Meteorologische Zeitschrift* **22**, 5–33.

- Wagner W, Lemoine G, Borgeaud M and Rott H** (1999a) A study of vegetation cover effects on ERS scatterometer data. *IEEE Transactions on Geoscience and Remote Sensing* **37**, 938–948.
- Wagner W, Lemoine G and Rott H** (1999b) A method for estimating soil moisture from ERS scatterometer and soil data. *Remote Sensing of Environment* **70**, 191–207.
- Wagner W, Pathe C, Doubkova M, Sabel D, Bartsch A, Hasenauer S, Bloschl G, Scipal K, Martinez–Fernandez J and Low A** (2008) Temporal Stability of Soil Moisture and Radar Backscatter Observed by the Advanced Synthetic Aperture Radar (ASAR). *Sensors* **8**, 1174–1197.
- Walker JP, Willgoose GR and Kalma JD** (2004) In-situ measurement of soil moisture: a comparison of techniques. *Journal of Hydrology* **293**, 85–99.
- Webster R and Oliver M** (2007) *Geostatistics for Environmental Scientists: 2. Edition*. Wiley. Available online from: www.perlego.com/book/2760842/geostatistics-for-environmental-scientists-pdf (Accessed 7 June 2024).
- Weir P and Dahlhaus P** (2023) In search of pragmatic soil moisture mapping at the field scale: A review. *Smart Agricultural Technology* **6**, 100330.
- Willmott CJ and Matsuura K** (2005) Advantages of the mean absolute error (MAE) over the root mean square error (RMSE) in assessing average model performance. *Climate Research* **30**, 79–82.
- Xaver A, Zappa L, Rab G, Pfeil I, Vreugdenhil M, Hemment D and Dorigo WA** (2020) Evaluating the suitability of the consumer low–cost Parrot Flower Power soil moisture sensor for scientific environmental applications. *Geoscientific Instrumentation, Methods Data Systems* **9**, 117–139.
- Zaussinger F, Dorigo W, Gruber A, Tarpanelli A, Filippucci P and Brocca L** (2019) Estimating irrigation water use over the contiguous United States by combining satellite and reanalysis soil moisture data. *Hydrology and Earth System Sciences* **23**, 897–923.

Zhang YH, Li HY, Sun YG, Zhang Q, Liu PZ, Wang R and Li J (2022) Temporal stability analysis evaluates soil water sustainability of different cropping systems in a dryland agricultural ecosystem. *Agricultural Water Management* **272**, 107834.

Zhou H, Geng G, Yang J, Hu H, Sheng L and Lou W (2022) Improving Soil Moisture Estimation via Assimilation of Remote Sensing Product into the DSSAT Crop Model and Its Effect on Agricultural Drought Monitoring. *Remote Sensing* **14**, 3187

Accepted Manuscript

Table 1. The four soil classes according to the available water capacity (AWC), area percentage and natural agriculture soil value in the test field

Soil class	Available soil water capacity up to 1 m [mm]	Soil layers [cm]	PWP [vol.%]	FC [vol.%]	Area percentage in the field [%]	Natural agriculture soil value ¹
Soil 1	138	0-20	15	36.5	20.5	medium-value arable land
		20-40	19.5	37.2		
		40-100	19.5	29.5		
Soil 2	174	0-20	16	43	35.3	medium-value arable land
		20-40	13	36.7		
		40-100	13	25.1		
Soil 3	196	0-20	25	47.5	37.6	high-quality arable land
		20-40	22.8	42.3		
		40-100	22.8	41.4		
Soil 4	220	0-20	11	39	6.6	high-quality arable areas
		20-40	11.3	36		
		40-100	11.3	30.3		

PWP, permanent wilting point; FC, field capacity
¹according to eBod (www.bodenkarte.at).

Table 2. Statistical analyses of Parrot-measured soil moisture (SM) vs. SM simulated by AquaCrop at 0–10 cm and DSSAT at 0–10 cm soil depth according to the 4 soil classes (MBE = mean bias error; MAE = mean absolute error; ubRMSE = unbiased root mean square error; KGE = Kling–Gupta efficiency; adj R² = adjusted coefficient of determination)

Soil class	MBE [vol.%]	MAE [vol.%]	ubRMSE [vol.%]	KGE [unitless]	adj R ² [unitless]
AquaCrop					
Soil 1	-6.14	6.26	3.18	0.78	0.88***
Soil 2	-0.47	4.45	5.12	0.75	0.76***
Soil 3	4.99	5.13	3.05	0.8	0.89***
Soil 4	-8.7	9.14	5.41	0.69	0.75***
DSSAT					
Soil 1	-4.96	5.36	3.07	0.76	0.93***
Soil 2	0.7	5.12	5.74	0.48	0.89***
Soil 3	5.22	5.81	5.35	0.51	0.87***
Soil 4	-5.67	6.33	4.12	0.73	0.9***

Signif. codes: P -value < 0.001 '***' (highly significant); $0.001 \leq P$ -value < 0.01 '**' (very significant); $0.01 \leq P$ -value < 0.05 '*' (significant); $0.05 \leq P$ -value < 0.1 '.' (marginally significant); P -value ≥ 0.1 ' ' (not significant).

Table 3. Statistical analyses of Parrot-measured soil moisture (SM) (averaged over the field) vs. SM simulated by AquaCrop at 0–10 cm and DSSAT at 0–10 cm soil depth (area-weighted values of all four soil classes; MBE = mean bias error; MAE = mean absolute error; ubRMSE = unbiased root mean square error; KGE = Kling–Gupta efficiency)

Crop model	MBE [vol.%]	MAE [vol.%]	ubRMSE [vol.%]	KGE [unitless]
AquaCrop	-0.12	3.15	3.87	0.87
DSSAT	0.82	4.17	4.84	0.6

Accepted Manuscript

Table 4. Statistical analyses of the Parrot-measured soil moisture (SM) vs. ARIS model-simulated SM (relative soil saturation) RSS 0–10 (soil depth 0-10cm), RSS 0–20 (soil depth 0-20cm), RSS 0–40 (soil depth 0-40cm) and remote sensing-derived SM (soil water index) SWI 01 (time delay 1), SWI 05 (time delay 5), and SWI 10 (time delay 10); SM values are converted into standard scores [unitless] (MBE = mean bias error; MAE = mean absolute error; ubRMSE = unbiased root mean square error; KGE = Kling–Gupta efficiency)

ARIS/RS	MBE	MAE	ubRMSE	KGE
RSS 0–10	-0.006	0.32	0.39	0.84
RSS 0–20	-0.018	0.32	0.41	0.58
RSS 0–40	-0.047	0.58	0.7	-0.06
SWI 01	-0.0007	0.49	0.65	0.77
SWI 05	0.006	0.35	0.43	0.83
SWI 10	0.002	0.52	0.62	0.78

ARIS model-simulated soil moisture: RSS = relative soil saturation; RS (remote sensing)-derived soil moisture; SWI = Soil Water Index

a)



b)

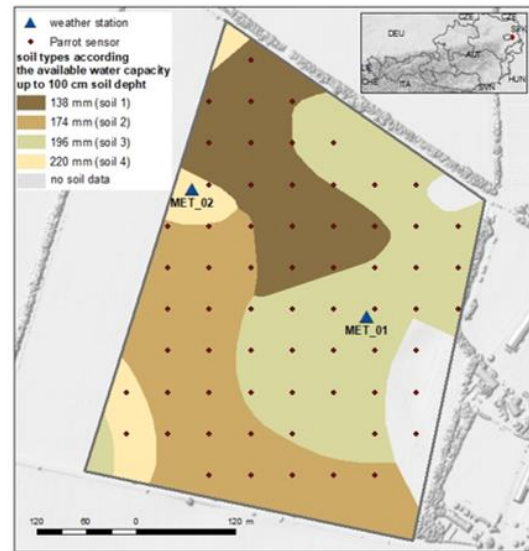


Figure 1. (a) Spatial representation of the soil surface colour (related to the sand content at the surface) and variability (Hymap, Marchfeld) within the field and test area (white framed) on 20/06/2006 (Eitzinger *et al.*, 2009; project DROSMON). (b) In situ measurement grid (50×50 m) of Parrot sensors, the locations of the two weather stations and the soil classes of the water capacity of the top layer 0–100 cm available for crops, derived from the eBod soil map, at the Rutzendorf test field (17 ha).

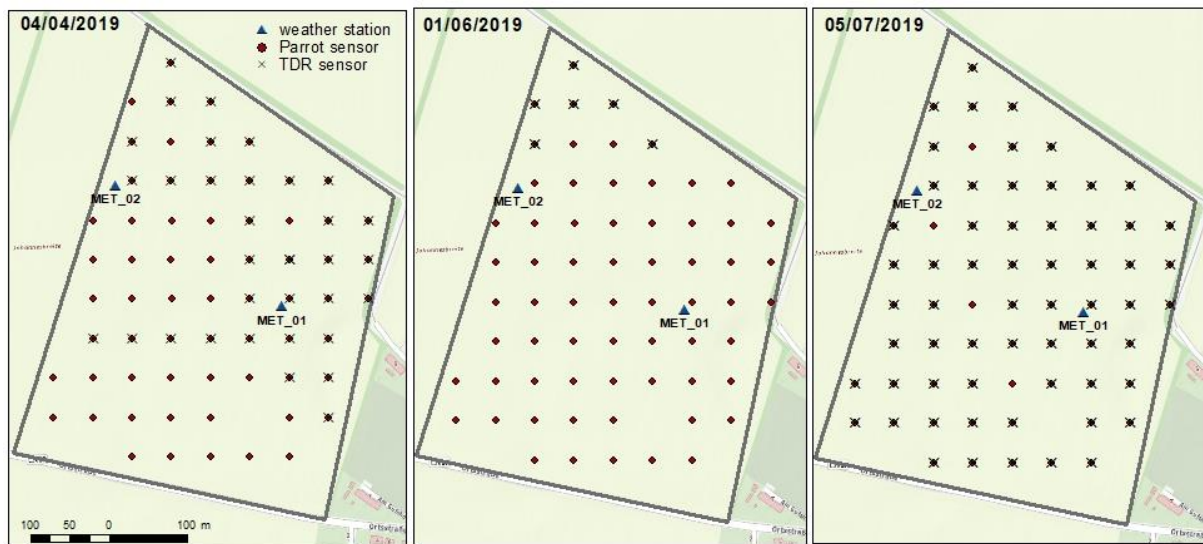


Figure 2. *In situ* measurement grid (50×50 m) of Parrot sensors and grid points of the reference TDR sensor measurements on 04/04/2019, 01/06/2019 and 05/07/2019.

Accepted Manuscript

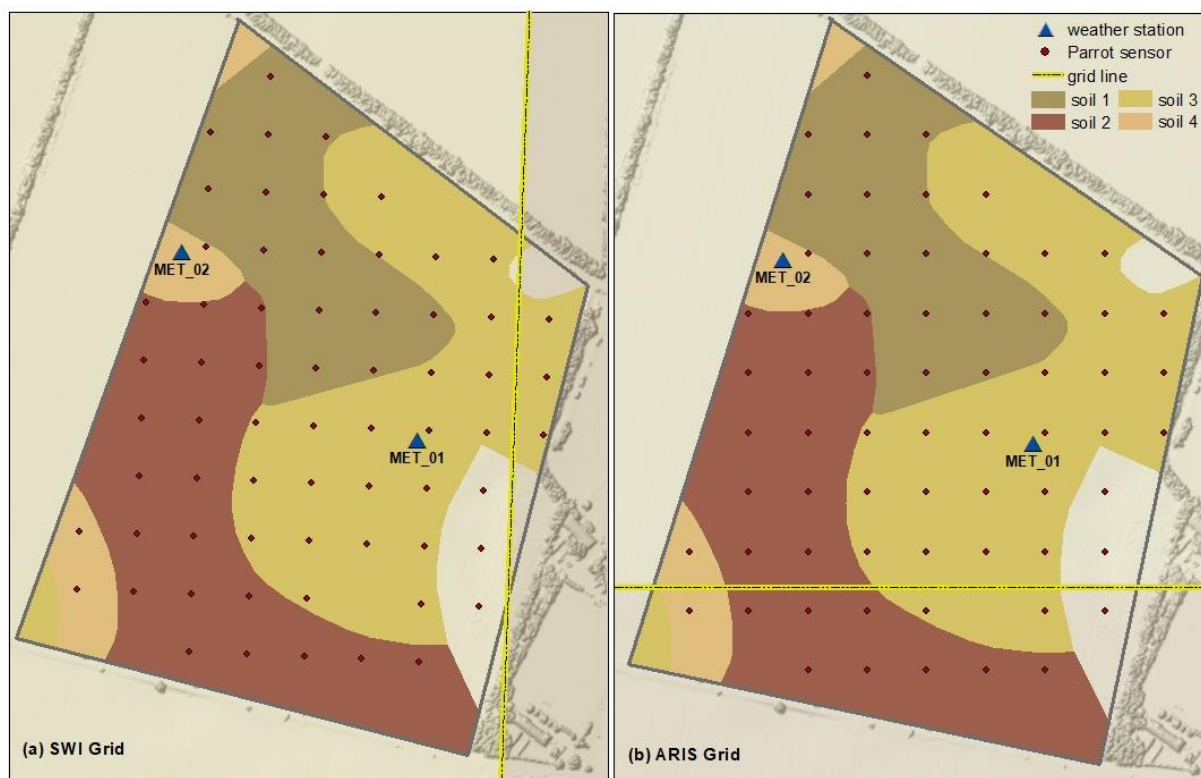
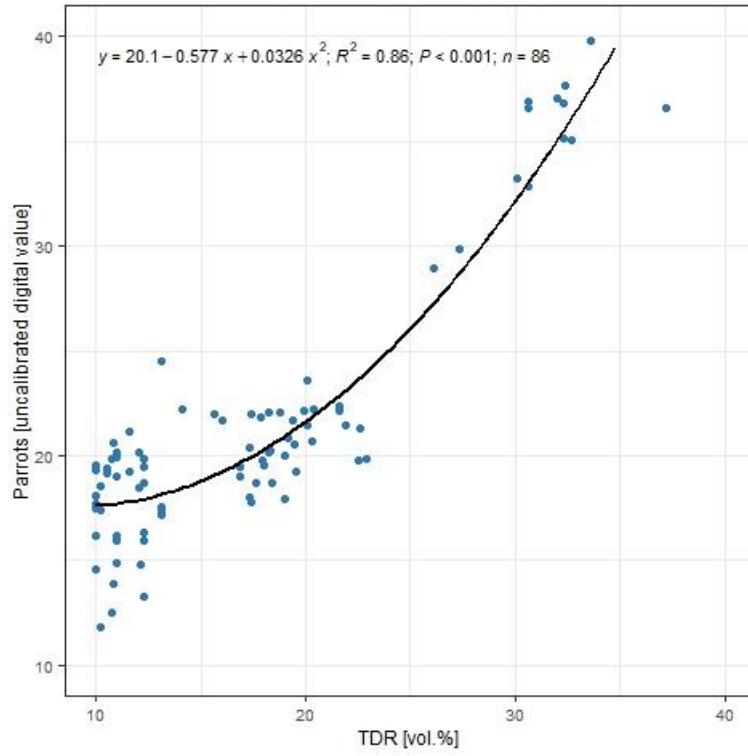


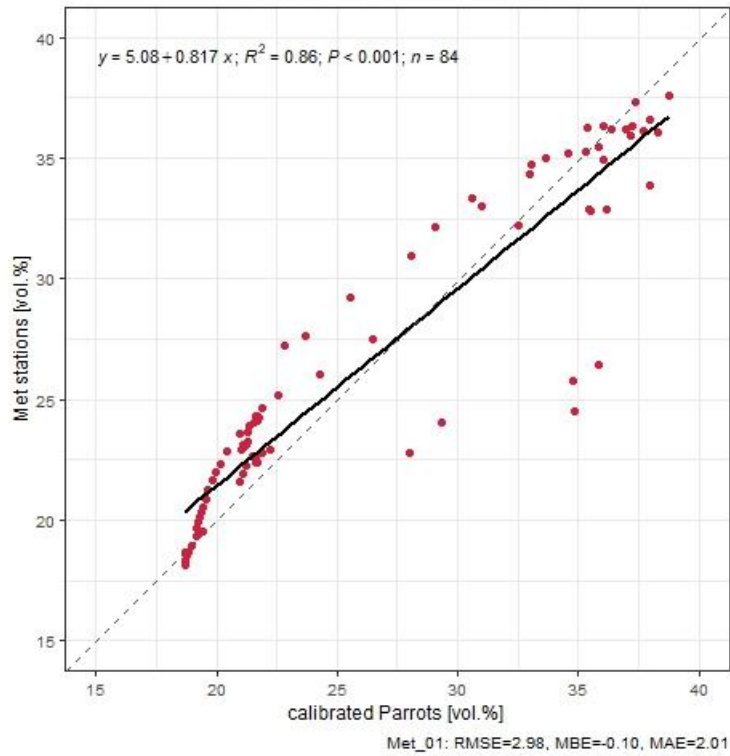
Figure 3. Grids overlapping with the field test site of 500 m: (a) remote sensing-derived soil moisture (SM) (SWI) and (b) ARIS model-simulated SM (RSS).

Accepted Manuscript

(a) TDR vs. uncalibrated Parrot



(b) calibrated Parrot vs. Met_01



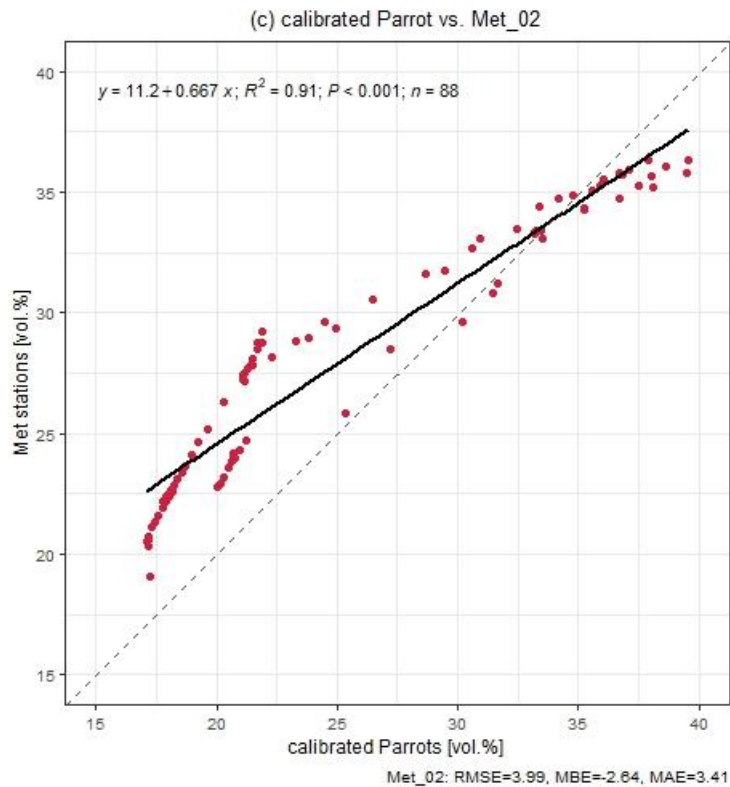


Figure 4. (a) Polynomial regression of soil moisture (SM) time-domain reflectometer (TDR) [vol.%] vs. uncalibrated Parrot sensors (0–10 cm soil depth), including R^2 (coefficient of determination); (b) linear regression of SM [vol.%] calibrated Parrot sensors (0–10 cm soil depth) vs. weather station Met_01 (0–30 cm soil depth), including R^2 , root mean square error (RMSE), mean bias error (MBE) and mean absolute error (MAE). The dashed line represents the 1:1 line; (c) linear regression of SM [vol.%] calibrated Parrot sensors (0–10 cm soil depth) vs. weather station Met_02 (0–20 cm soil depth), including R^2 , RMSE, MBE and MAE. The dashed line represents the 1:1 line.

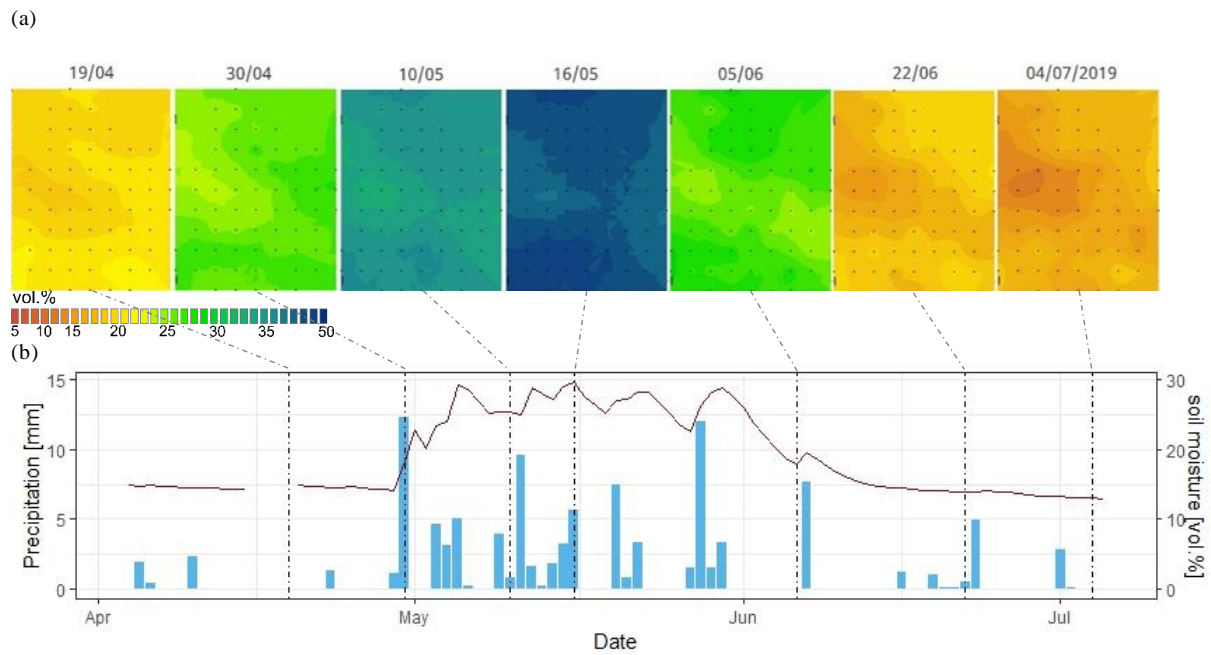


Figure 5. (a) Spatial variability of soil moisture (SM) [vol.%] across the experimental field at Rutzendorf on 19/04, 30/04, 10/05, 16/05, 05/06, 22/06 and 04/07/2019, as determined by kriging. The dots represent the in-situ Parrot measurement points. (b) Daily precipitation [mm, bars] and mean SM content [vol.%, line] determined by Parrot measurements at the experimental field in Rutzendorf from 04/04 to 05/07/2019; the dotted lines represent the days of the SM map shown above.

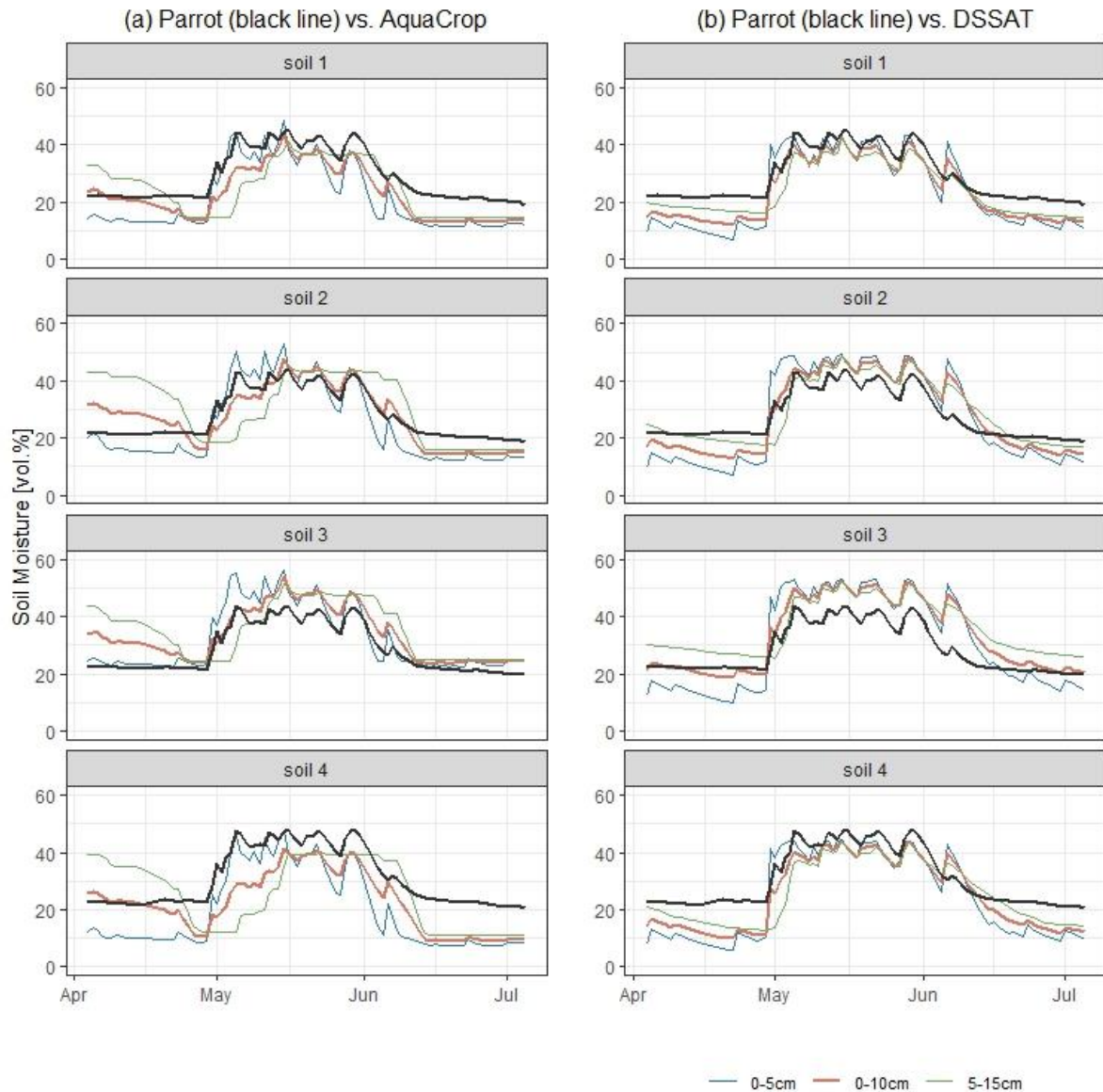


Figure 6. Soil moisture [vol.%] time series from the Parrot sensors (black line) vs. (a) AquaCrop and (b) DSSAT (soil depth 0–5 cm blue line, 0–10 cm red line, 5–15 cm green line) according to the 4 soil types during the wheat spring growing season in 2019.

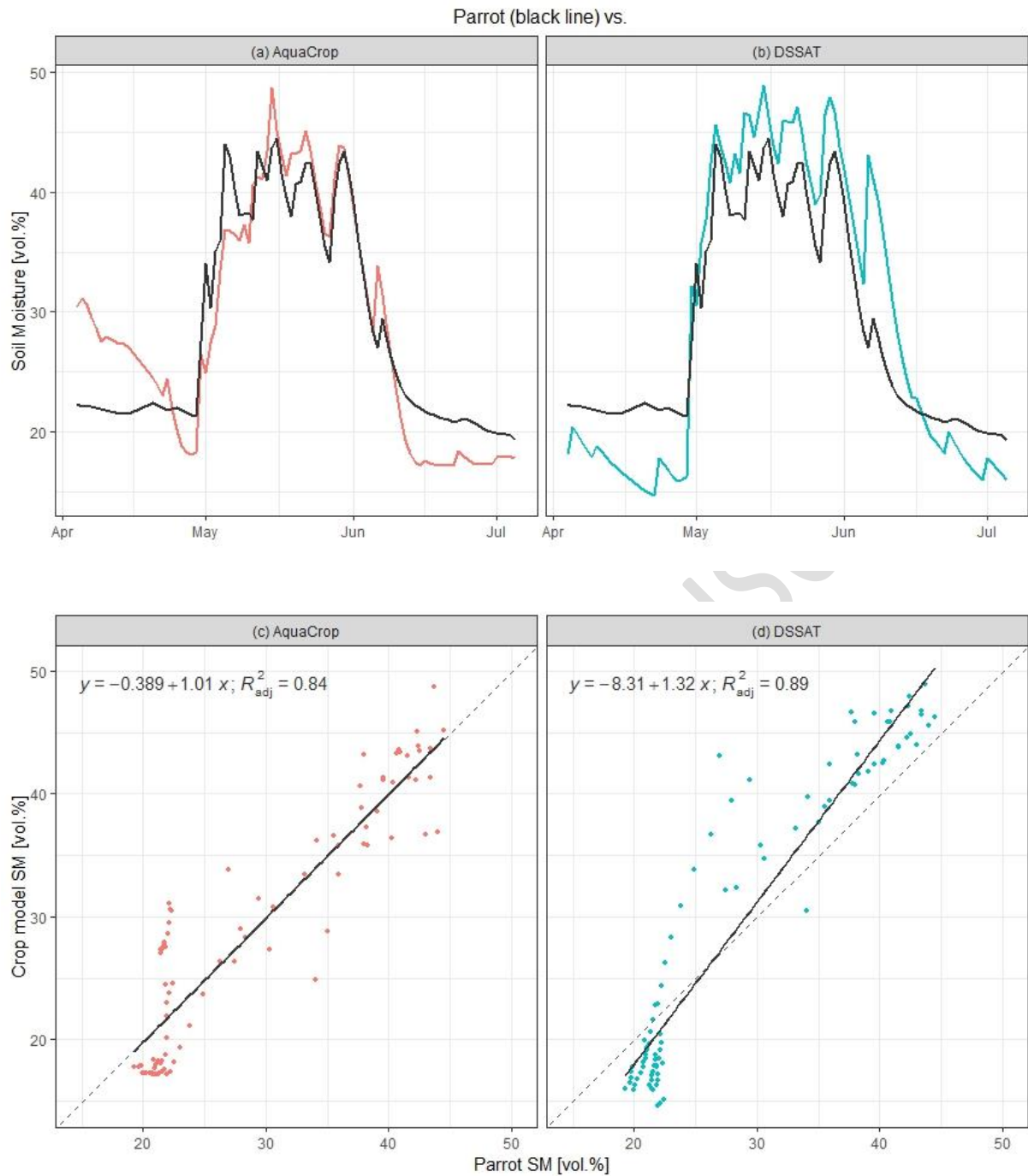


Figure 7. Soil moisture (SM) [vol.%] time series from the Parrot sensors (black line) vs. (a) AquaCrop (red line) and (b) DSSAT (blue line) (soil depth 0–10 cm) during the wheat spring growing season in 2019 (average value over the experimental field); linear regression and R^2 of SM [vol.%] Parrot vs. (c) AquaCrop and (d) DSSAT; the dashed line represents the 1:1 line.

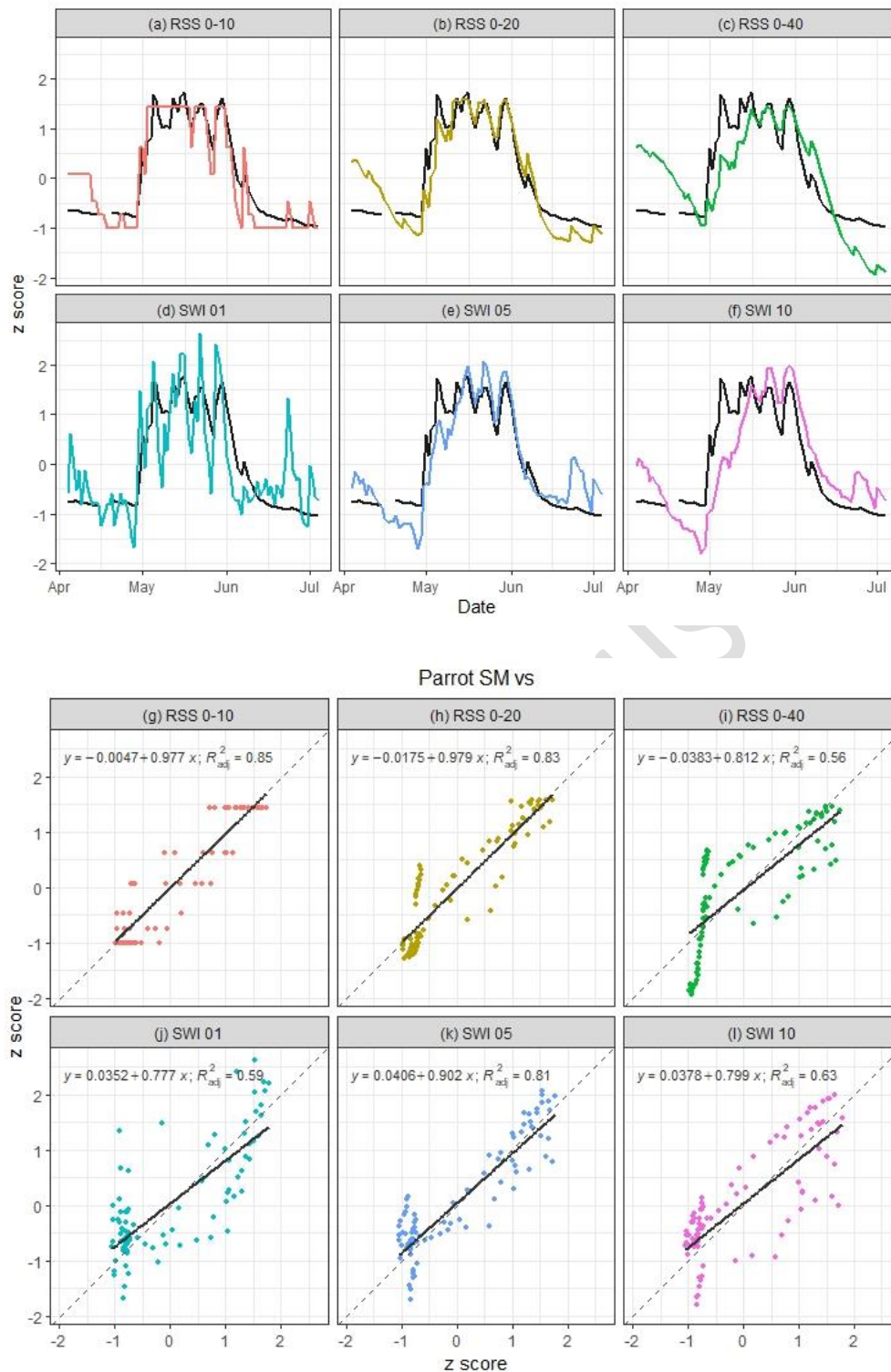


Figure 8. Soil moisture (SM) time series from the Parrot sensors (black line) vs. ARIS model-simulated SM (relative soil saturation) (a) RSS 0–10 (soil depth 0–10cm), (b) RSS 0–20 (soil depth 0–20cm), (c) RSS 0–40 (soil depth 0–40cm) and remote sensing-derived SM (soil water index) (d) SWI 01 (time delay 1), (e) SWI 05 (time delay 5), and (f) SWI 10 (time delay 10); linear regression and R^2 of Parrot vs. (g) RSS 0–10, (h) RSS 0–20, (i) RSS 0–40, (j) SWI 01,

(k) SWI 05, and (l) SWI 10; the dashed line represents the 1:1 line (SM values are converted into standard scores).

Accepted Manuscript